ADA033887

(12)

THE FLUID MECHANICS OF PULSED LASER PROPULSION

FINAL REPORT

A. N. Pirri, G. A. Simons and P. E. Nebolsine

July 1976

Prepared for

DEFENSE ADVANCED RESEARCH PROJECTS AGENCY
Arlington, VA 22209
ARPA Order 3176

Monitored by

OFFICE OF NAVAL RESEARCH
Department of the Navy
Arlington, VA 22217
Contract No. N00014-76-C-0738

PHYSICAL SCIENCES INC.
30 COMMERCE WAY, WOBURN, MASS. 01801

UNCLASSIFIED

SECURITY CLASSIFICATION OF THIS PAGE (When Data Entered)

REPORT DOCUMENTATION PAGE		READ INSTRUCTIONS BEFORE COMPLETING FORM
1. REPORT NUMBER	2. GOVT ACCESSION NO.	3. RECIPIENT'S CATALOG NUMBER
4. TITLE (and Subtitle) 6 THE FLUID MECHANICS OF PULSED LASER PROPULSION.		5. TYPE OF REPORT & PERIOD COVERED FINAL Report Period 3/1/76 - 6/30/76
		6. PERFORMING ORG. REPORT NUMBER 14 PSI-TR-60
7. AUTHOR(s) 10 A. N. Pirri, G. A. Simons ~~and~~ P. E. Nebolsine		8. CONTRACT OR GRANT NUMBER(s) 15 N00014-76-C-0738, ARPA Order-3176
9. PERFORMING ORGANIZATION NAME AND ADDRESS Physical Sciences Inc. 30 Commerce Way Woburn, MA 01801		10. PROGRAM ELEMENT, PROJECT, TASK AREA & WORK UNIT NUMBERS ARPA Order No. 3176
11. CONTROLLING OFFICE NAME AND ADDRESS Office of Naval Research Department of the Navy Arlington, VA 22217		12. REPORT DATE 11 31 July ~~31,~~ 1976
		13. NUMBER OF PAGES 12 93 p.
14. MONITORING AGENCY NAME & ADDRESS (if different from Controlling Office) 9 Final rept. 1 Mar - 30 Jun 76,		15. SECURITY CLASS. (of this report) Unclassified
		15a. DECLASSIFICATION/DOWNGRADING SCHEDULE

16. DISTRIBUTION STATEMENT (of this Report)

Distribution Unlimited; approved for public release

17. DISTRIBUTION STATEMENT (of the abstract entered in Block 20, if different from Report)

18. SUPPLEMENTARY NOTES

19. KEY WORDS (Continue on reverse side if necessary and identify by block number)

laser propulsion	laser effects
radiatively heated flows	advanced propulsion concepts
detonation propulsion	

20. ABSTRACT (Continue on reverse side if necessary and identify by block number)

A fluid mechanical model is developed to assess the performance of a rocket that is propelled by the absorption of radiant energy from a remotely stationed, repetitively pulsed laser. The model describes the flow within a conical nozzle that is subjected to point energy depositions at the apex of the cone. A similarity solution is obtained and the specific impulse and energy efficiencies that may

DD FORM 1 JAN 73 1473 EDITION OF 1 NOV 65 IS OBSOLETE

UNCLASSIFIED

SECURITY CLASSIFICATION OF THIS PAGE (When Data Entered)

391105 Dn

be achieved with such a device are determined. Fluid mechanical constraints limit the range of pulse repetition rates that may be utilized. Preliminary design considerations indicate that a specific impulse of 800 seconds or greater may be achieved with both a laboratory and a full scale device. A two pound laboratory rocket can be accelerated at 10 g's with a 15 joule laser pulsed 25,000 times per second. A one ton rocket will require a megajoule laser operating at 350 pulses per second to achieve an equivalent acceleration.
A laboratory experiment to test the theoretical model using multiple CO_2 TEA lasers is also designed, and a test plan to compare theory with experiment is outlined.

PSI TR-60

THE FLUID MECHANICS OF PULSED LASER PROPULSION

A. N. Pirri, G. A. Simons and P. E. Nebolsine

July 31, 1976

Final Report

Period 1 March 1976 - 30 June 1976

Prepared for

DEFENSE ADVANCED RESEARCH PROJECTS AGENCY
1400 Wilson Boulevard
Arlington, VA 22209
ARPA Order 3176

Monitored by

OFFICE OF NAVAL RESEARCH
Department of the Navy
800 N. Quincy Street
Arlington, VA 22217

Contract No. N00014-76-C-0738

ACKNOWLEDGEMENT

This research was supported by the Advanced Research Projects Agency of the Department of Defense and was monitored by Office of Naval Research under Contract No. N00014-76-C-0738.

The authors would like to acknowledge David Rosen for his assistance in the experiment design and Irene Scanzillo for preparation of the report.

MISSING PAGE
NUMBERS ARE BLANK
AND WERE NOT
FILMED

ABSTRACT

A fluid mechanical model is developed to assess the performance of a rocket that is propelled by the absorption of radiant energy from a remotely stationed, repetitively pulsed laser. The model describes the flow within a conical nozzle that is subjected to point energy depositions at the apex of the cone. A similarity solution is obtained and the specific impulse and energy efficiencies that may be achieved with such a device are determined. Fluid mechanical constraints limit the range of pulse repetition rates that may be utilized. Preliminary design considerations indicate that a specific impulse of 800 seconds or greater may be achieved with both a laboratory and a full scale device. A two pound laboratory rocket can be accelerated at 10 g's with a 15 joule laser pulsed 25,000 times per second. A one ton rocket will require a megajoule laser operating at 350 pulses per second to achieve an equivalent acceleration. A laboratory experiment to test the theoretical model using multiple CO_2 TEA lasers is also designed, and a test plan to compare theory with experiment is outlined.

TABLE OF CONTENTS

		Page
	ABSTRACT	iii
I.	INTRODUCTION	1
II.	SINGLE PULSE THEORY	7
III.	DEFINITIONS FOR MULTIPLE PULSE THEORY	15
IV.	MULTIPLE PULSE THEORY	19
V.	OPERATIONAL LIMITATIONS	29
VI.	NOZZLE AND PLENUM PRESSURE TRACES	43
VII.	EXPERIMENT DESIGN	49
VIII.	SUMMARY AND CONCLUSIONS	65
	REFERENCES	67
	APPENDIX	A-1

LIST OF ILLUSTRATIONS

			Page
Fig. 1	a)	Single Pulse Propulsion Concept as Introduced in Ref. 4	4
	b)	Multiple Pulse Propulsion Concept and Equivalent Conical Nozzle	4
Fig. 2		Density Profile Behind Strong Shock	11
Fig. 3		Pressure Profile Behind Strong Shock	12
Fig. 4		Velocity Profile Behind Strong Shock	13
Fig. 5	a)	Critical Pulse Time	21
	b)	Shock "Breakthrough" Time ($t_p < t_c$)	21
Fig. 6		Integral Properties of the Similarity Solution	24
Fig. 7		Enhancement of Specific Impulse Due to Pulsed Energy Addition	25
Fig. 8		Specific Impulse	27
Fig. 9		Thrust Reduction Due to Flow Divergence	30
Fig. 10		Thrust Reduction Due to Finite Length Nozzles	33
Fig. 11		Thrust Reduction Due to Finite Ambient Pressure	35
Fig. 12		Rocket Size Requirements	37

		Page
Fig. 13	Laser Power Requirements	38
Fig. 14	Laser Energy Requirements	39
Fig. 15	Laser Energy Vs. Pulse Repetition Frequency	41
Fig. 16	Pressure Behind Nozzle Shock	44
Fig. 17	Pressure Time History in Throat	45
Fig. 18	Pulsed Laser Propulsion Experiment Schematic with Parabolic Nozzle	50
Fig. 19	Laser Power and Pulse Repetition Rate Vs. Rocket Thrust	52
Fig. 20	Example of Spark Technique for Measuring Exhaust Velocity from Ref. 15	54
Fig. 21	Conical Nozzle Design	57
Fig. 22	Parabolic Nozzle Design	59
Fig. 23	Test Matrix	62
Fig. A-1	Idealized Nozzle Curvature	A-2
Fig. A-2	Distribution of Thrust in η Space	A-3
Fig. A-3	Acoustic Waves Propagating From Corner	A-6
Fig. A-4	Radial Motion of Loading Wave	A-9
Fig. A-5	Angular Motion of Leading Wave	A-10
Fig. A-6	Angular Motion of Trailing Wave	A-11

		Page
Fig. A-7	Maximum PLP Degradation (Shock B)	A-16
Fig. A-8	Shock B Degradation For $\sigma_{wall} = 30^{o}$	A-17
Fig. A-9	PLP Degradation - Shock A	A-22
Fig. A-10	Total Degradation for 30^{o} Wall	A-23

I. INTRODUCTION

In recent years, several authors[1-7] have discussed and analyzed the possibility of beamed laser energy for rocket propulsion, often with specific reference to the application of high power, ground-based lasers. The concept is deceptively simple: provide a high energy density for propulsion without the encomberance of a massive on-board power supply by absorbing radiation from a remotely stationed high-power laser. Since the radiation absorbing propellant may be a high temperature plasma, the specific impulse can be very large. The achievable thrust may only be limited by the available laser power, and with a remote energy source large payload/vehicle weight ratios are possible.

A series of experiments to determine the specific impulse and thrust/laser power that can be obtained with existing laser systems are described in Ref. 4. Steady-state simulation experiments were performed in a vacuum chamber with solid propellants, and pulsed laser propulsion along with the laser-powered pulse jet concept is introduced. A steady-state or CW laser propulsion system is a system whose thrust remains constant in time while the laser beam continuously provides the energy source for converting propellant mass to exhaust kinetic energy. It was found in Ref. 4 that a high ratio of thrust to laser power can be obtained by simply using the laser to vaporize a solid surface. However, in order to obtain high specific impulse it is necessary to add energy to the vapor in a stable manner. The heating of a gas by external radiation downstream of a nozzle throat was found to be inherently unstable when the gas is initially weakly ionized and absorbs radiation via inverse Bremsstrahlung. The stability of laser-heated flows both upstream and

downstream of a nozzle throat is not adequately understood and is a very complex issue.[7] However, it appears that stable heating of a propellant in a steady state manner may best be accomplished by heating the gas upstream of a throat such that the beam direction and the propellant flow direction are the same. This would require a laser window in the absorption chamber that will tolerate transmission of significant laser intensities along with high pressures for long periods of time.

The alternative approach to laser propulsion that circumvents the stability problem is to utilize a pulsed laser. The techniques for obtaining large thrust and specific impulse with a pulsed laser are an outgrowth of various experimental and theoretical programs in laser effects.[8-12] When a high power pulsed laser is focused to a high intensity in a gas or on a solid surface, a high temperature, high pressure plasma, which propagates up the laser beam, is initiated. Provided the pulse is sufficieitnly short that the high pressure gas remains in the vicinity of a surface or nozzle wall, this method may be an efficient propulsion mechanism. The propulsion system operates in a way similar to detonation propulsion systems that have been proposed for use in high pressure environments.[13] Periodic "explosions" in the nozzle transfer the detonation or laser energy to the working fluid. The two most significant potential advantages afforded by a pulsed laser propulsion system over a CW laser propulsion system are 1) simplicity in engine design as a result of permitting the laser beam to enter the nozzle via the exhaust plane, and 2) elimination of constraints resulting from plasma instability. However, the power conversion efficiency (efficiency of converting laser power to power in the rocket exhaust) must be determined. In Ref. 4 a low power conversion efficiency was obtained because the pulse time of the laser was too long. In addition, with pulsed laser propulsion,

thrust is obtained when laser energy is converted to kinetic energy by a continuously weakening shock wave traversing the propellant gas. The relative efficiency of generating thrust in this manner is not known a priori to be the same as when converting laser power to thrust in a steady process.

The purpose of the present report is a detailed study of the fluid mechanics of pulsed laser propulsion. As a result of this theoretical study the laser requirements for an experimental test of pulsed laser propulsion concepts are specified, and a suggested experiment is presented. The objective is to determine the relative efficiency of a pulsed laser propulsion system compared to a CW system and to calculate the specific impulse and thrust as a function of laser power, pulse repetition frequency, ambient conditions and propellant mass flow. The nozzle configuration is taken to be an idealized extension of the concept introduced in Refs. 2 and 4. A schematic of the single pulse nozzle configuration[2,4] is presented in Fig. 1a. The nozzle walls focus the incoming beam to yield a breakdown in the air at the focus. With a short laser pulse, the resulting shock becomes a blast wave which propagates to the nozzle exit plane, converting all of the high pressure gas behind it into a force on the nozzle wall. This nozzle was designed for single pulse operation only. Therefore, no considerations of propellant supply were necessary. In this report the fluid mechanics of a repetitively pulse laser propulsion system is analyzed, and thus, the fluid dynamics of the propellant feed system is included. The configuration to be analyzed is shown in Fig. 1b. The nozzle drawn with a solid line is the parabolic self focusing nozzle. However, for simplicity this nozzle is replaced by a conical nozzle which is shown dashed in the figure. The angle of the cone is chosen such that the exhaust gases leave the exit plane at the same angle relative to the thrust axis as with the parabolic nozzle. The beam is assumed to be focused externally so that the focusing angle equals the cone angle. The propellant is treated as a steady source flow entering at the apex or "throat" of the conical nozzle, and periodically

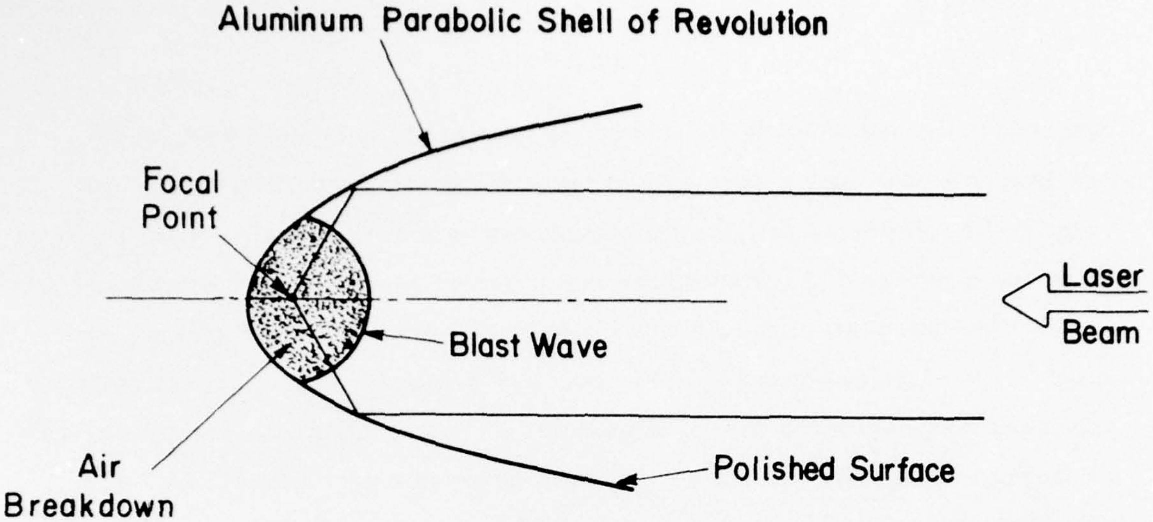

(a)

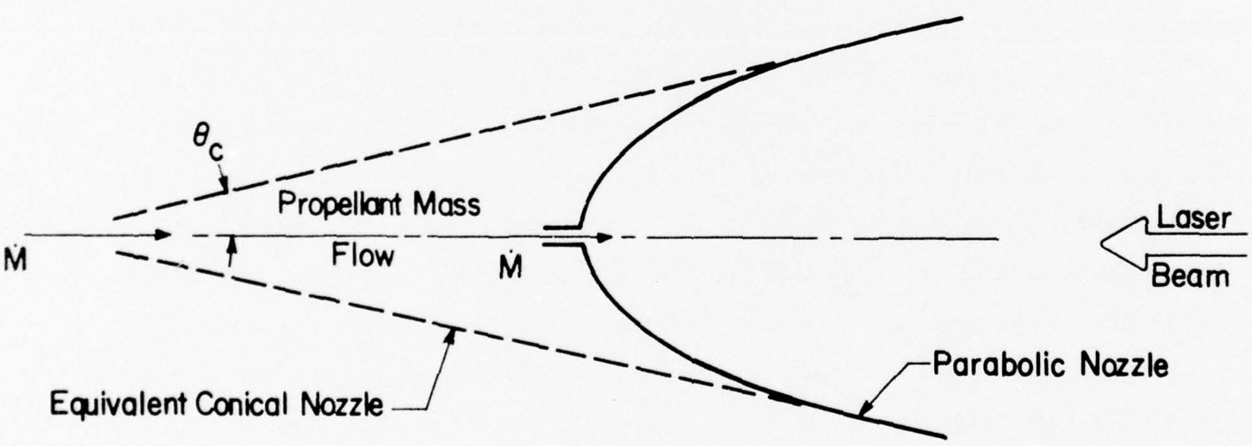

(b)

Fig. 1 a) Single Pulse Propulsion Concept as Introduced in Ref. 4

b) Multiple Pulse Propulsion Concept and Equivalent Conical Nozzle

laser induced blast waves are ignited at $r = 0$ where r is measured from the apex. In Sec. II the theory for single pulse propulsion, where the propellant gas expands into a vacuum, is presented. Sections III and IV describe the extension of the analysis to multiple pulses to determine the specific impulse and thrust as a function of pulse repetition frequency. A discussion of operational limitations such as the effects of the cone angle, a finite exit plane back pressure, propellant plenum chamber conditions and nozzle curvature is included in subsequent sections. The design of an experiment to test the theory of pulsed laser propulsion is presented in Section VII.

II. SINGLE PULSE THEORY

Consider the steady propellant flow through a conical nozzle of solid angle Ω. Utilizing spherical symmetry within that solid angle, we obtain the gas density ρ_1

$$\rho_1 = \rho^* (r^*)^2 / \sqrt{\frac{\gamma + 1}{\gamma - 1}}\ r^2 \tag{1}$$

where ρ^* is the density at sonic conditions, r is the spherical radius and r^* is the radius of the hypothetical "source" of strength $\dot{M}$,

$$\dot{M} = \rho^* u^* (r^*)^2 \Omega ,$$

where u^* is the sonic gas velocity. The gas velocity in the supersonic portion of the nozzle is assumed to be the limiting velocity of the gas at zero temperature.

$$u_1 = u_\ell = \sqrt{\frac{\gamma + 1}{\gamma - 1}}\ u^* \tag{2}$$

Equations (1) and (2) represent the gas density and velocity downstream of the source radius r^*. There is a local failure of the equations for $r \leq 0(r^*)$. However, mass flux is conserved within this radius.

At $t = 0$ we shall (with a pulsed laser) deposit energy E at $r = 0$. This energy will generate a shock wave which propagates with velocity $V_s(t)$ spherically outward to radius $R_s(t)$. Equations (1) and (2) represent the conditions upstream of the shock. Therefore, the shock propagates into a gas whose density $\sim 1/r^2$. It has already been assumed that u_ℓ is much greater than the upstream speed of sound. Hence, if we assume that

$V_s >> u_\ell$, the shock may be considered strong in the traditional sense of the strong blast wave.[14] The density, pressure, and gas velocity immediately behind the shock become

$$\rho_s(t) = \left(\frac{\gamma+1}{\gamma-1}\right)\rho_1 = \sqrt{\frac{\gamma+1}{\gamma-1}}\;\rho^*(r^*)^2/R_s^2(t) ,$$

$$p_s(t) = \left(\frac{2}{\gamma+1}\right)\rho_1 V_s^2(t) = \frac{2}{(\gamma+1)}\sqrt{\frac{\gamma-1}{\gamma+1}}\;\rho^*(r^*)^2 V_s^2(t)/R_s^2(t) ,$$

and
$$u_s(t) = \left(\frac{2}{\gamma+1}\right)V_s(t) ,$$

respectively.

In order to obtain the density, pressure and velocity everywhere between $r = 0$ and $r = R_s(t)$, we must solve the inviscid Euler equations. The conservation of mass, momentum and energy are, respectively:

$$\frac{\partial\rho}{\partial t} + \frac{\partial(\rho u)}{\partial r} + \frac{2\rho u}{r} = 0 ,$$

$$\frac{\partial u}{\partial t} + u\frac{\partial u}{\partial r} + \frac{1}{\rho}\frac{\partial p}{\partial r} = 0 , \tag{3}$$

and
$$\frac{\partial(p/\rho^\gamma)}{\partial t} + u\frac{\partial(p/\rho^\gamma)}{\partial r} = 0 .$$

We seek a solution to Eqs. (3) for the blast wave propagating into a nonuniform gas that is similar in $r/R_s(t)$. That is, we assume

$$\rho = \rho_s(t)\, f(\eta),$$

$$p = p_s(t)\, g(\eta),$$

and

$$u = u_s(t)\, h(\eta) \ ,$$

where

$$\eta = r/R_s(t) \ .$$

Substituting the self-similar profiles into the Euler equations, we determine the shock motions for which the variables η and t may be separated:

$$R_s(t) = A t^m \ , \qquad (4)$$

where A and m are arbitrary constants. The thermal and kinetic energy in the shocked gas must be equal to the energy deposited at $r = 0$.

$$E = \int_0^{R_s(t)} (C_v T + \frac{1}{2} u^2)\, \rho\, \Omega\, r^2\, dr \qquad (5)$$

From Eqs. (4) and (5), it follows that

$$m = 2/3$$

and

$$A = \left(E / \rho^* (r^*)^2\, \Omega\, I_1\right)^{1/3}$$

where

$$I_1 = \frac{8 \int_0^1 (g + f h^2)\, \eta^2\, d\eta}{9\,(\gamma + 1)\sqrt{(\gamma+1)}\sqrt{(\gamma - 1)}} \ .$$

Equation (4) is valid for the time period over which the shock is strong. The limiting time is the time at which the shock velocity decays to the upstream gas velocity. This is denoted by t_{max} and is determined from

$$V_s(t_{max}) = u_\ell$$

or

$$t_{max} = \frac{8E\left(\frac{\gamma-1}{\gamma+1}\right)^{3/2}}{27\,\Omega\, I_1\, \rho^*\, (r^*)^2\, (u^*)^3} \quad . \tag{6}$$

Having successfully separated the η and t variables, the resulting equations for the conservation of mass, momentum and energy become, respectively,

$$h' = \left(\frac{\gamma+1}{2}\right)\frac{\eta f'}{f} + (\gamma+1) - \frac{2h}{\eta} - \frac{hf'}{f} \quad ,$$

$$g' = \frac{1}{2}\left(\frac{\gamma+1}{\gamma-1}\right) hf + \left(\frac{\gamma+1}{\gamma-1}\right) f \left(\eta - \frac{2h}{(\gamma+1)}\right) h' \quad , \tag{7}$$

and

$$(\gamma - 3/2)\,(\gamma+1)\; g + \left(h - \frac{(\gamma+1)\eta}{2}\right)\left(g' - \frac{\gamma g f'}{f}\right) = 0 \; .$$

Equations (7) are integrated from $\eta = 1$ to $\eta = 0$, subject to the condition that

$$h\,(1) = g\,(1) = f\,(1) = 1 \quad .$$

The density, pressure and velocity profiles are illustrated in Figs. 2, 3 and 4 respectively. These solutions will be utilized to determine the performance of a pulsed laser propelled rocket.

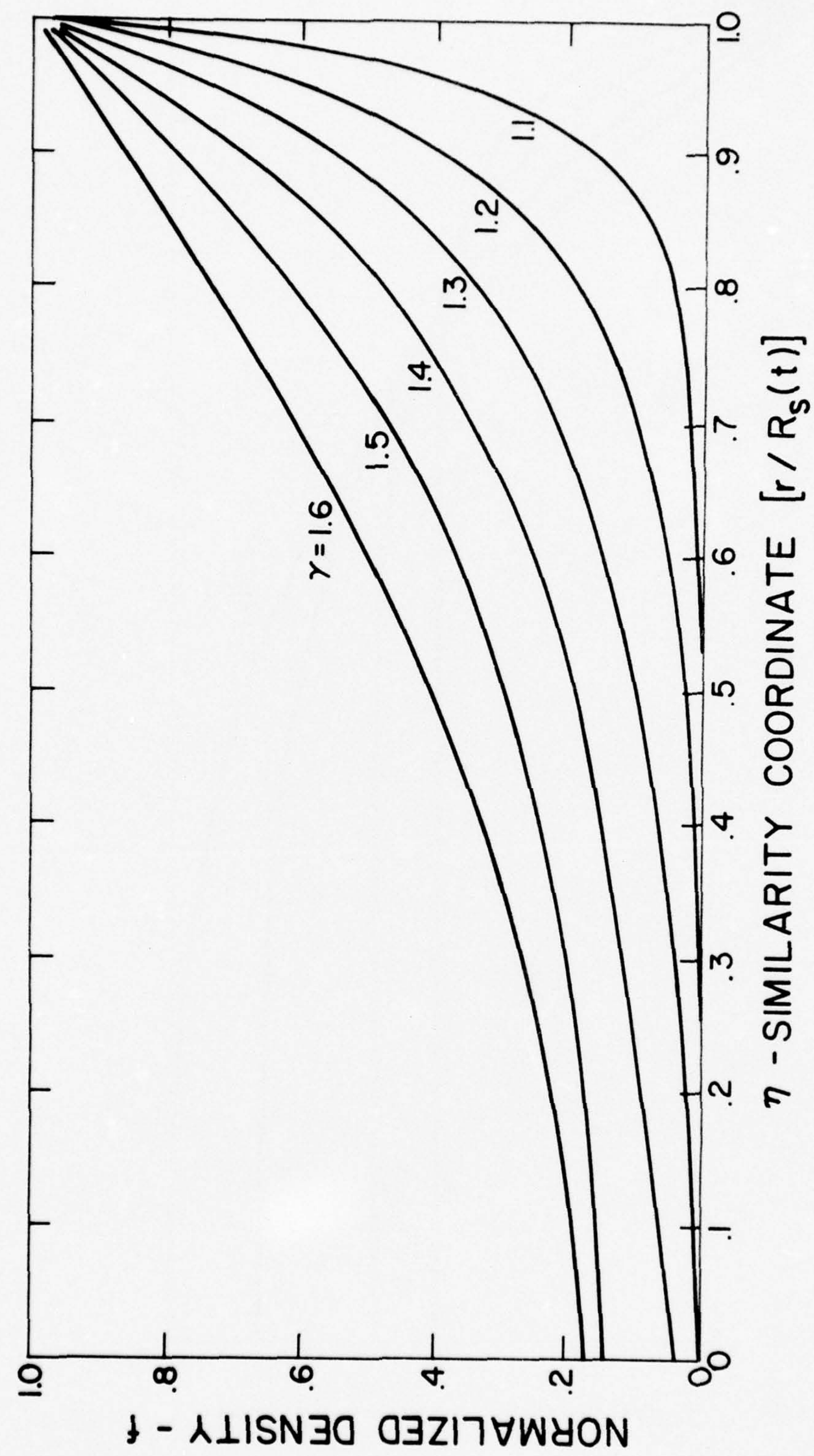

Fig. 2 Density Profile Behind Strong Shock

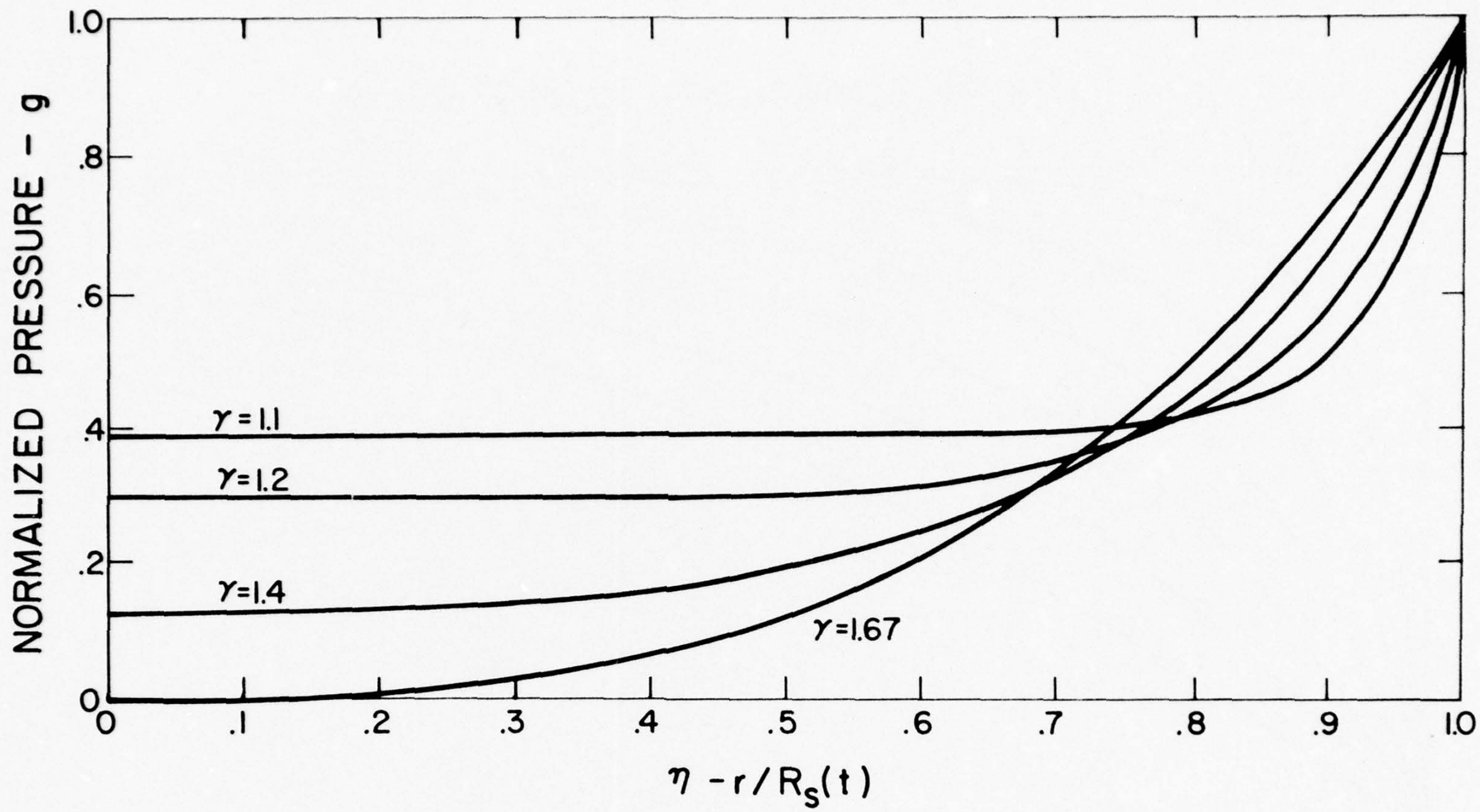

Fig. 3 Pressure Profile Behind Strong Shock

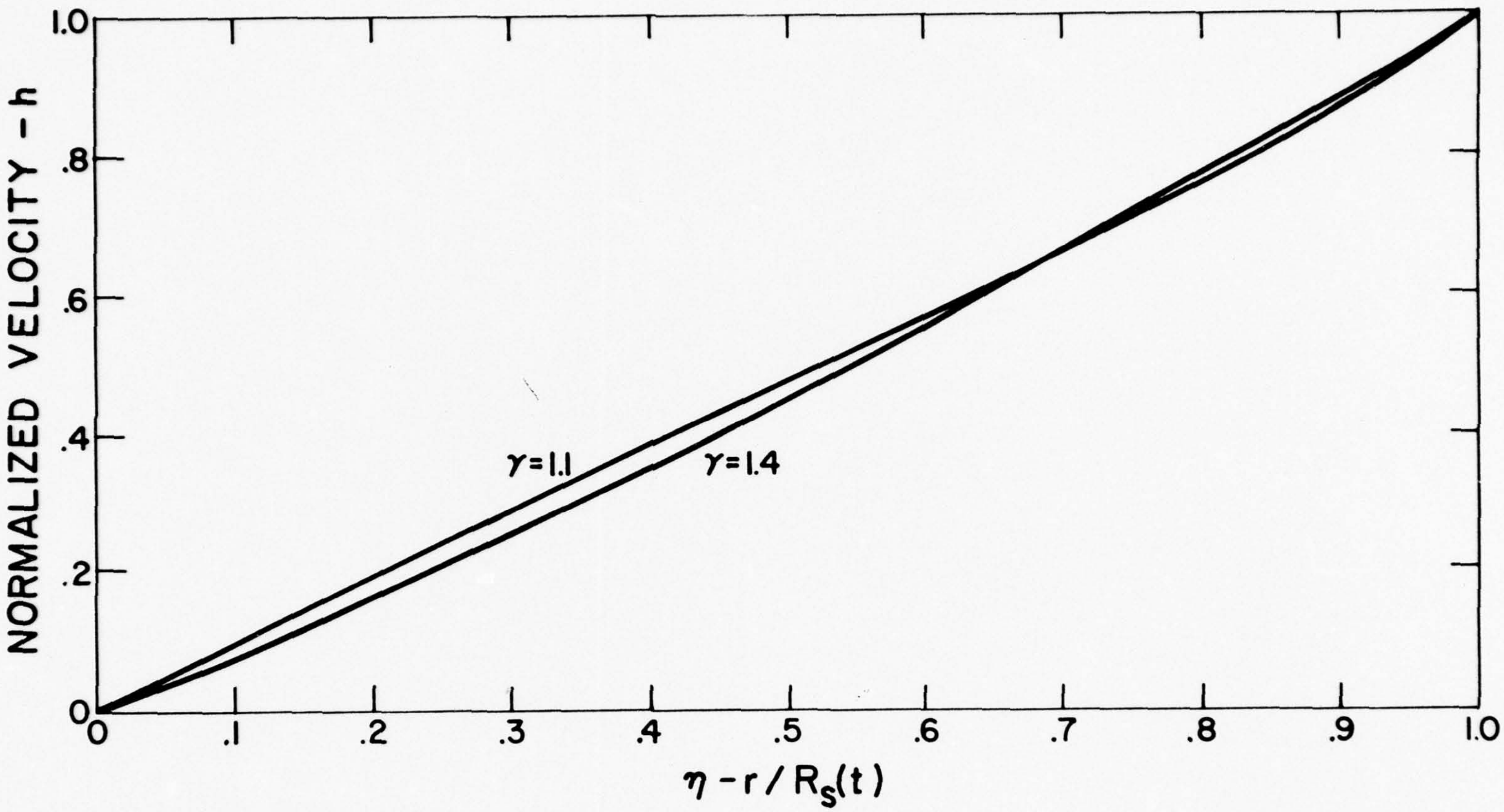

Fig. 4 Velocity Profile Behind Strong Shock

III. DEFINITIONS FOR MULTIPLE PULSE THEORY

Before extending the fluid mechanical model to include pulse sequencing, we will first define and relate the time average quantities in a notation similar to that used for conventional rockets.

Consider a pulsed laser propulsion system in which mass M is released per cycle and t_p is the time between pulses (in contrast to the pulse duration). The time average mass flux, thrust and power are defined by

$$\overline{\dot{M}} = M/t_p \ ,$$

$$\overline{T} = \frac{1}{t_p} \int_0^{t_p} T\,dt \ ,$$

and

$$\overline{P} = \frac{1}{t_p} \int_0^{t_p} P\,dt \ ,$$

respectively. The specific impulse, I_{sp}, is defined in terms of the time average thrust and mass flux

$$I_{sp} = \frac{\overline{T}}{\overline{\dot{M}}\,g} \ ,$$

where g is the acceleration of gravity. In addition to the time average quantities, it is necessary to define a mass average quantity. Denoting the nozzle exit plane velocity of the mass element dm as u_e, we express the mass average exit plane velocity as

$$\overline{u}_e = \frac{1}{M} \int_0^M u_e\,dm \ . \tag{8}$$

We seek to determine the optimum thrust $\bar{T}$ for the minimum time average laser power $\bar{P}$.* In the limit of zero temperature at the exit plane, the instantaneous thrust T is related to $\bar{u}_e$ by

$$\int_o^{t_p} T\,dt = M\bar{u}_e ,$$

and the instantaneous laser power P is related to the kinetic energy by

$$\int_o^{t_p} P\,dt = (1/2)\,M\bar{u}_e^{\,2} \int_o^1 \left(\frac{u_e}{\bar{u}_e}\right)^2 d\left(\frac{m}{M}\right) .$$

From the above relations, the ratio of thrust to power is expressed as

$$\frac{\bar{T}}{\bar{P}} = \frac{2/\bar{u}_e}{\int_o^1 \left(\frac{u_e}{\bar{u}_e}\right)^2 d\left(\frac{m}{M}\right)} .$$

and the mass average exit plane velocity is related to the specific impulse via

$$I_{sp} = \bar{u}_e/g . \tag{9}$$

Eliminating $\bar{u}_e$ between Eqs. (19) and (20), the ratio of thrust to power becomes

$$\frac{\bar{T}}{\bar{P}} = \frac{2\,e_R}{g\,I_{sp}} ,$$

---

*Note that the time average laser power is the average continuous power delivered by a repetitively pulsed device. The peak laser power is the average power delivered over the duration of the laser pulse. The latter concept is not used in this report

where e_R is defined as the relative efficiency and is expressed as

$$e_R = \left[\int_o^1 \left(\frac{u_e}{\bar{u}_e} \right)^2 d \left(\frac{m}{M} \right) \right]^{-1} \tag{10}$$

The quantity e_R is a measure of the energy efficiency of a pulsed device relative to a continuous working (CW) or steady state device. For CW laser propulsion, a steady flow system is obtained and the exit plane velocity is the same for all mass elements. Hence, e_R is identically unity and the CW device is the reference state for the relative efficiency. From the mathematical definition of $\bar{u}_e$, it follows that

$$e_R \leq 1 .$$

To understand the physical meaning of the relative efficiency, consider a nozzle from which mass M/2 exits with velocity $V + \epsilon$ and mass M/2 exits with velocity $V - \epsilon$. The net momentum is MV but the energy required is $1/2 \, M(V^2 + \epsilon^2)$. Hence, the thrust to power is reduced with increasing non-uniformity ϵ. For pulsed laser propulsion, the energy deposition is not uniform and lower efficiencies will result. The fluid mechanical model for pulsed laser propulsion is now extended to include pulse sequencing and the relative efficiency of the pulsed device is assessed.

IV. MULTIPLE PULSE THEORY

The single pulse model just treated assumes that the source flow is established prior to the detonation at $r = 0$. The high pressure created by the blast will stop the source flow until such time that the pressure at $r = 0$ drops below the pressure of the sonic orifice. The time at which the point source again generates a finite mass flux is denoted by t_s^*, which, by definition, occurs when

$$p_s(t_s^*)\, g(0) = p^*$$

or

$$t_s^* = \frac{2}{3} \sqrt{g(0)} \sqrt{\frac{2\gamma}{\gamma+1)}} \left(\frac{\gamma - 1}{\gamma + 1}\right)^{1/4} r^*/u^* .$$

Numerical results (presented later in Fig. 6) indicate that t_s^* is significantly shorter than the time required for the gas to flow through the throat (r^*/u^*). We may wish to consider a mechanical delay in re-starting the point source. Hence, we define t_s as the time at which we mechanically allow the source to re-start.

$$t_s \geq t_s^*$$

Once the point source is re-started, the gas will expand with velocity u_ℓ into the relative vacuum created by the tail of the blast wave. At some time sufficiently greater than t_s, we wish to create a second pulse. Let us define the critical time (t_c) for the next pulse such that the shock would just propagate through the source gas when the shock itself becomes weak. A schematic diagram is presented in Fig. 5a to illustrate the meaning of t_c. The value of t_c is readily determined by balancing

the mass released by the source during the time interval $(t_c - t_s)$ with the mass swept out by the spherical shock as it passes through the source gas. Therefore,

$$\rho^* u^* (r^*)^2 \Omega (t_c - t_s) = \int_0^{t_{max}} \rho_1 V_s \Omega R_s^2 \, dt \quad ,$$

or

$$R_s (t_{max}) = (t_c - t_s) u_\ell \; .$$

Since t_{max} is defined by $V_s (t_{max}) = u_\ell$, it follows that

$$t_c - t_s = \frac{3}{2} t_{max} \; . \tag{11}$$

We wish to restrict the time between pulses (t_p) such that

$$t_p \leq t_c \quad , \tag{12}$$

otherwise, the shock will become weak before it propagates through all of the source gas and a lower specific impulse will result. For pulse repetition frequencies which satisfy Eq. (12), the shock will "break through" the source gas in a time (after detonation) less than t_{max}. Let us denote this time by t_b, as depicted in Fig. 5b.

We may evaluate t_b in a manner equivalent to that used in determining t_c. Mass balance again requires

$$R_s (t_b) = (t_p - t_s) u_\ell \quad , \tag{13a}$$

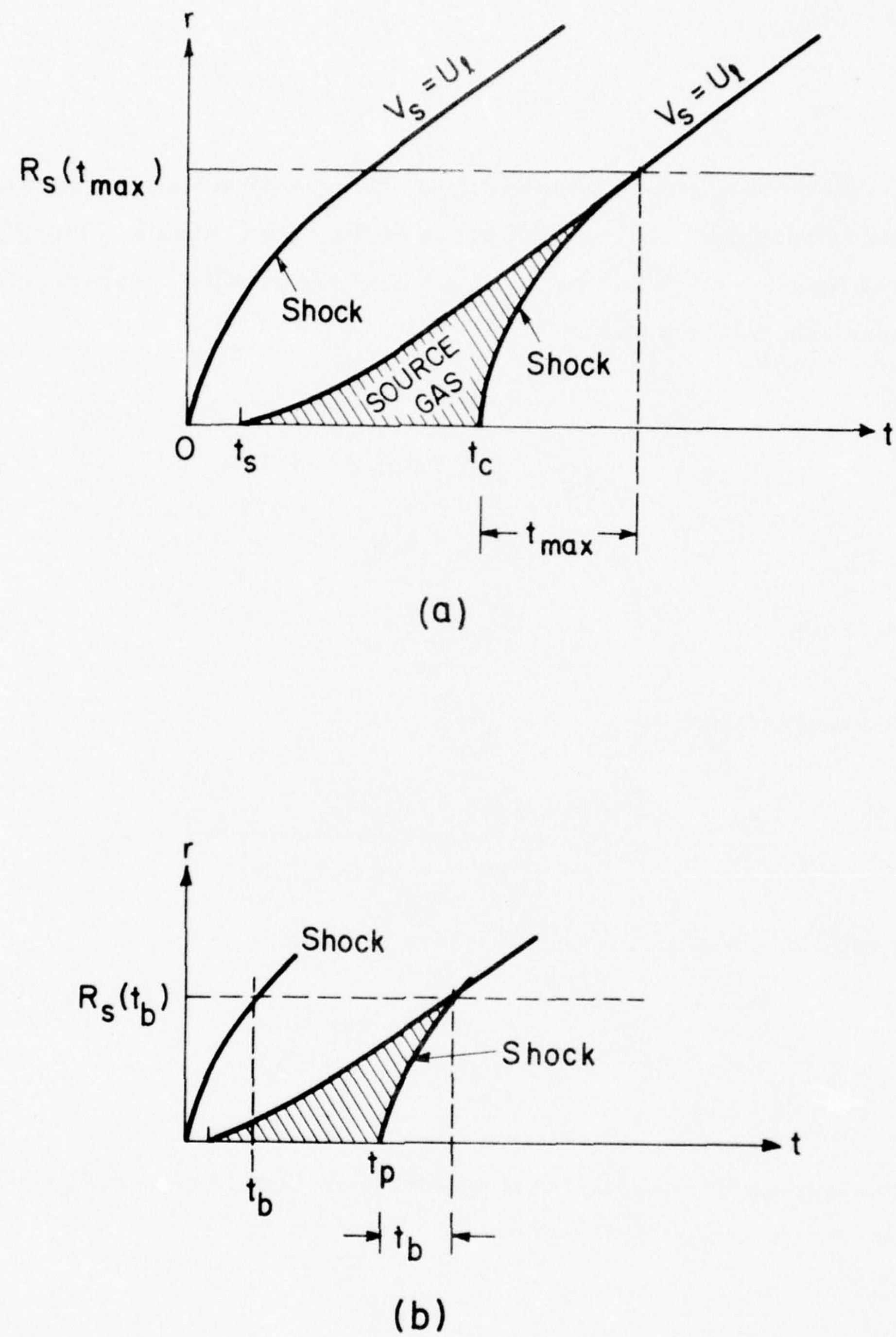

Fig. 5 a) Critical Pulse Time

b) Shock "Breakthrough" Time ($t_p < t_c$)

or

$$t_b = \left((t_p - t_s) \, u_\ell / A \right)^{3/2} . \tag{13b}$$

At time t_b (after detonation) we have a high pressure gas which must expand isentropically to the exit plane of the rocket nozzle. The gas is located between $r = 0$ and $r = R_s(t_b)$. The gas density, pressure and velocity are, respectively,

$$\rho_b = \rho_s(t_b) \, f(\eta_b) \quad ,$$

$$p_b = p_s(t_b) \, g(\eta_b) \quad ,$$

and

$$u_b = u_s(t_b) \, h(\eta_b)$$

where

$$\eta_b = r/R_s(t_b) \quad .$$

Each mass element dm,

$$\frac{dm}{M} = \frac{\Omega \, \rho_s(t_b) \, R_s^3(t_b) \, f(\eta_b) \, \eta_b^2 \, d\eta_b}{\rho^* u^* (r^*)^2 \, \Omega \, (t_p - t_s)} \quad ,$$

may expand to the maximum exit plane velocity

$$u_e = u_s(t_b) \sqrt{h^2(\eta_b) + \gamma \, g(\eta_b)/f(\eta_b)} \; ,$$

corresponding to zero temperature and pressure. The mass average exit plane velocity, Eq. (8) becomes

$$\overline{u}_e = \frac{2 \, I_2 \, u_\ell}{(\gamma - 1) \sqrt{\tau}} \quad , \tag{14}$$

where

$$\tau = \frac{t_p - t_s}{t_c - t_s} \quad ,$$

and

$$I_2 = \int_0^1 f\, \eta^2 \sqrt{h^2 + \gamma g/f}\; d\eta \ ,$$

where we have noted that the integrals over η_b and η are equivalent. From expressions for u_e and $\bar{u}_e$, Eq. (10) may be evaluated to determine the relative efficiency

$$e_R = \frac{(\gamma + 1)\ I_2^2}{(\gamma - 1)\ I_3} \ , \tag{15}$$

where

$$I_3 = \int_0^1 (f\, h^2 + \gamma g)\ \eta^2\ d\eta \quad .$$

Numerical results for e_R along with I_1, I_2, I_3 and $t_s\ u^*/r^*$ are illustrated in Fig. 6 and the results are very promising. For all practical purposes, the pulsed laser system is as efficient as the CW system. The reason for this result is that the bulk of the mass lies immediately behind the shock where the velocity is approximately the same for all mass elements. Hence, the relative efficiency, as defined by Eq. (10), is nearly unity.

Having shown that the pulsed laser propulsion concept is as efficient as the CW operation, we now use Eqs. (14) and (2) to determine the specific impulse.

$$\frac{I_{sp}}{(u_\ell / g)} = \frac{2\ I_2}{(\gamma - 1)\sqrt{\tau}} \tag{16}$$

The specific impulse is normalized to u_ℓ/g, the specific impulse of the source gas without energy addition, and the results are illustrated in Fig. 7. Note that $\tau < 1$ is required in order to obtain a specific impulse significantly greater than that of the source gas alone. This is consistent with the previously imposed constraint that t_p must be less than t_c.

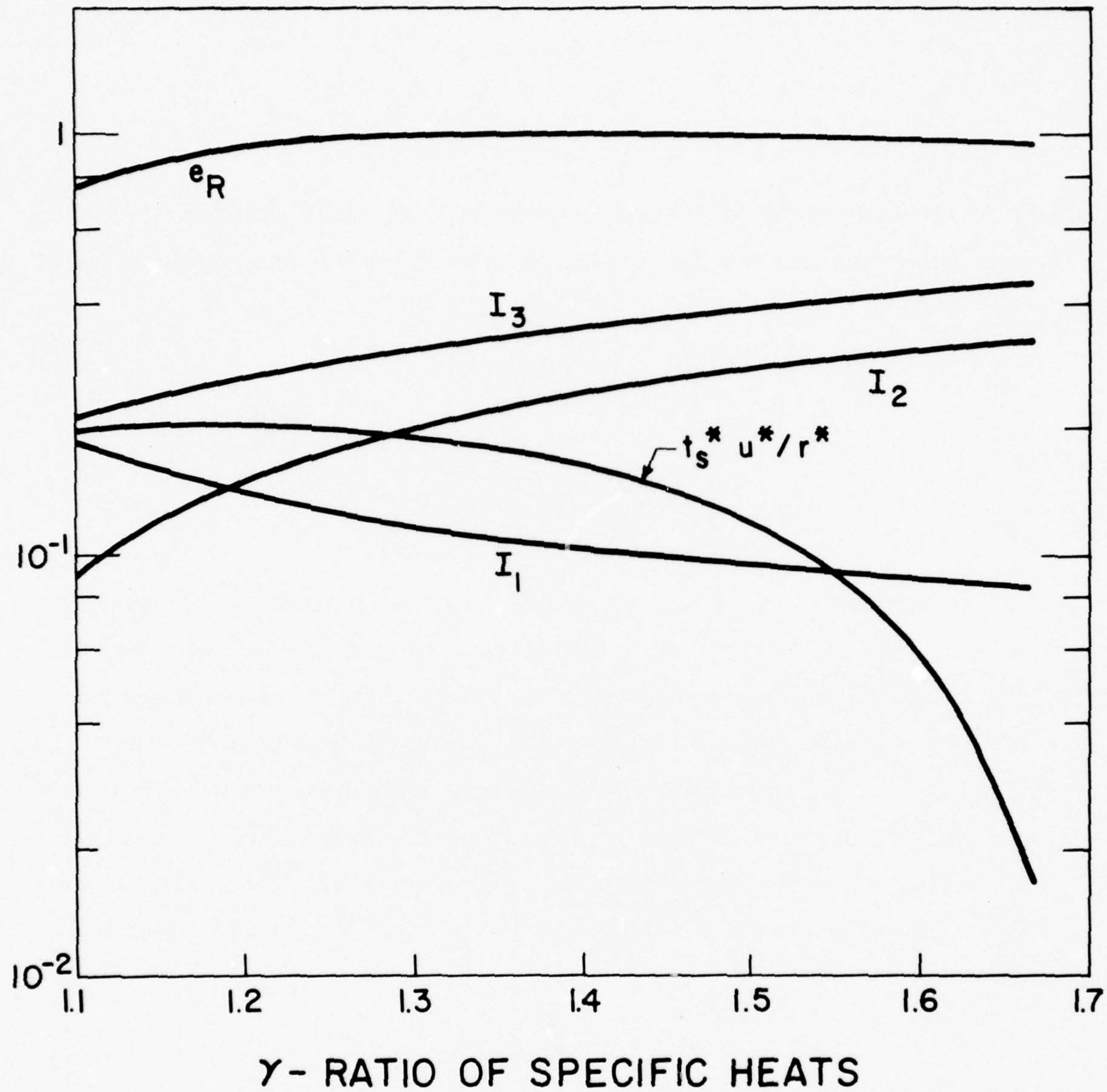

Fig. 6 Integral Properties of the Similarity Solution

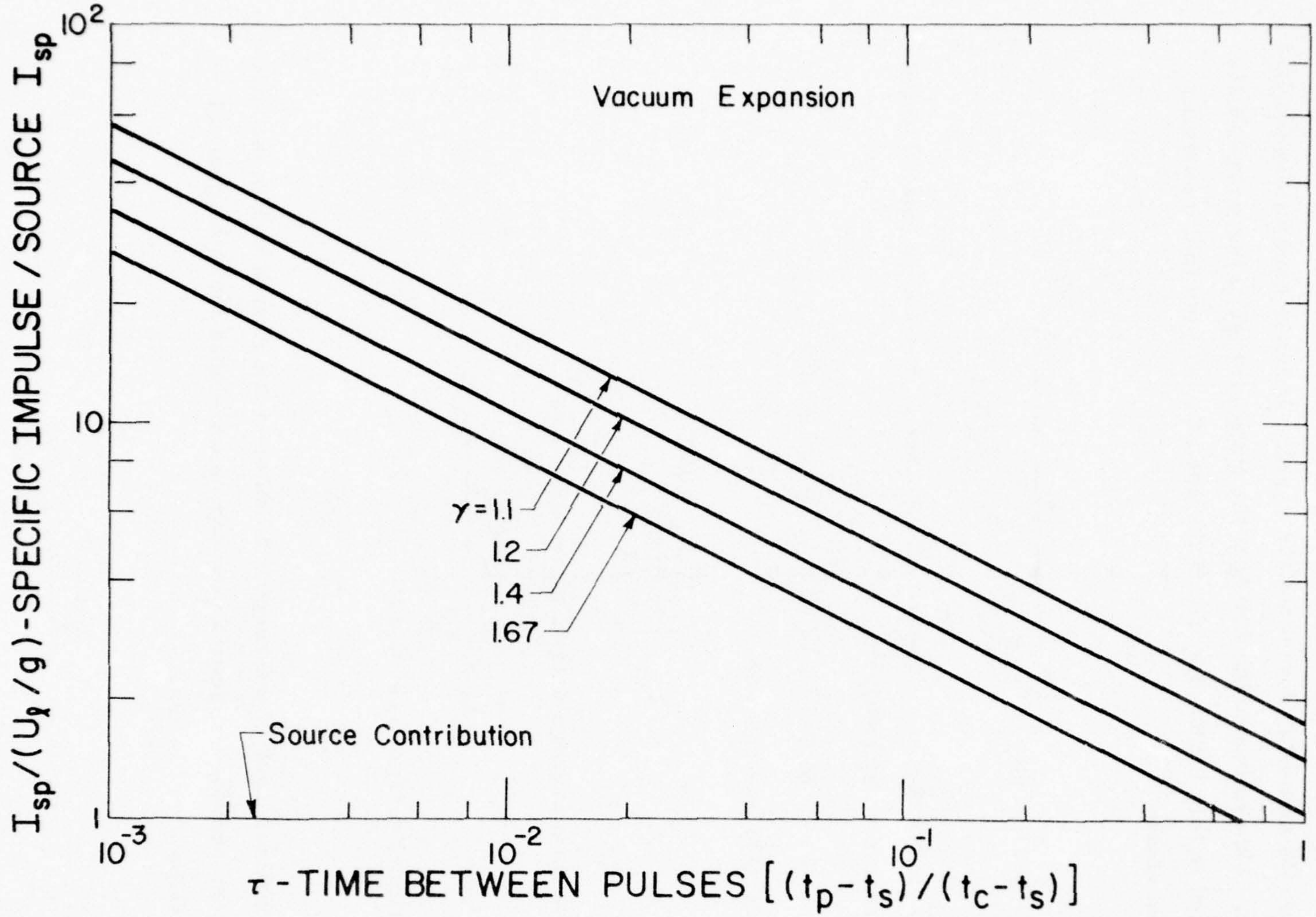

Fig. 7 Enhancement of Specific Impulse Due to Pulsed Energy Addition

Equation (16) also illustrates that the specific impulse becomes unbounded as $\tau \to 0$. This is due to the fact that the time average laser power is also unbounded in this limit. Rewriting the specific impulse in dimensional form, we obtain

$$I_{sp} = \frac{1.6}{g} \left(\frac{E}{\rho^* u^* (D^*)^2 (t_p - t_s)} \right)^{1/2} \qquad (17)$$

where D^* is the throat diameter of the rocket nozzle and is related to the source radius r^* by continuity,

$$\dot{M} = \rho^* u^* \Omega (r^*)^2 = \rho^* u^* \pi (D^*)^2 /4 \ .$$

From Eq. (17), we conclude

$$I_{sp} = \left(\frac{1.4}{g}\right)\left(\frac{\overline{P}}{\overline{\dot{M}}}\right)^{1/2} ,$$

where the time average mass flow is defined as

$$\overline{\dot{M}} = \frac{M}{t_p} = \frac{\dot{M}(t_p - t_s)}{t_p} ,$$

and the time average laser power is

$$\overline{P} = E/t_p \ .$$

The theoretical limit of the specific impulse is illustrated in Fig. 8. However, these results are general and can be developed from the general relationships given in Sec. III.

$$I_{sp} = \frac{\sqrt{2 e_R}}{g} \sqrt{\frac{\overline{P}}{\overline{\dot{M}}}}$$

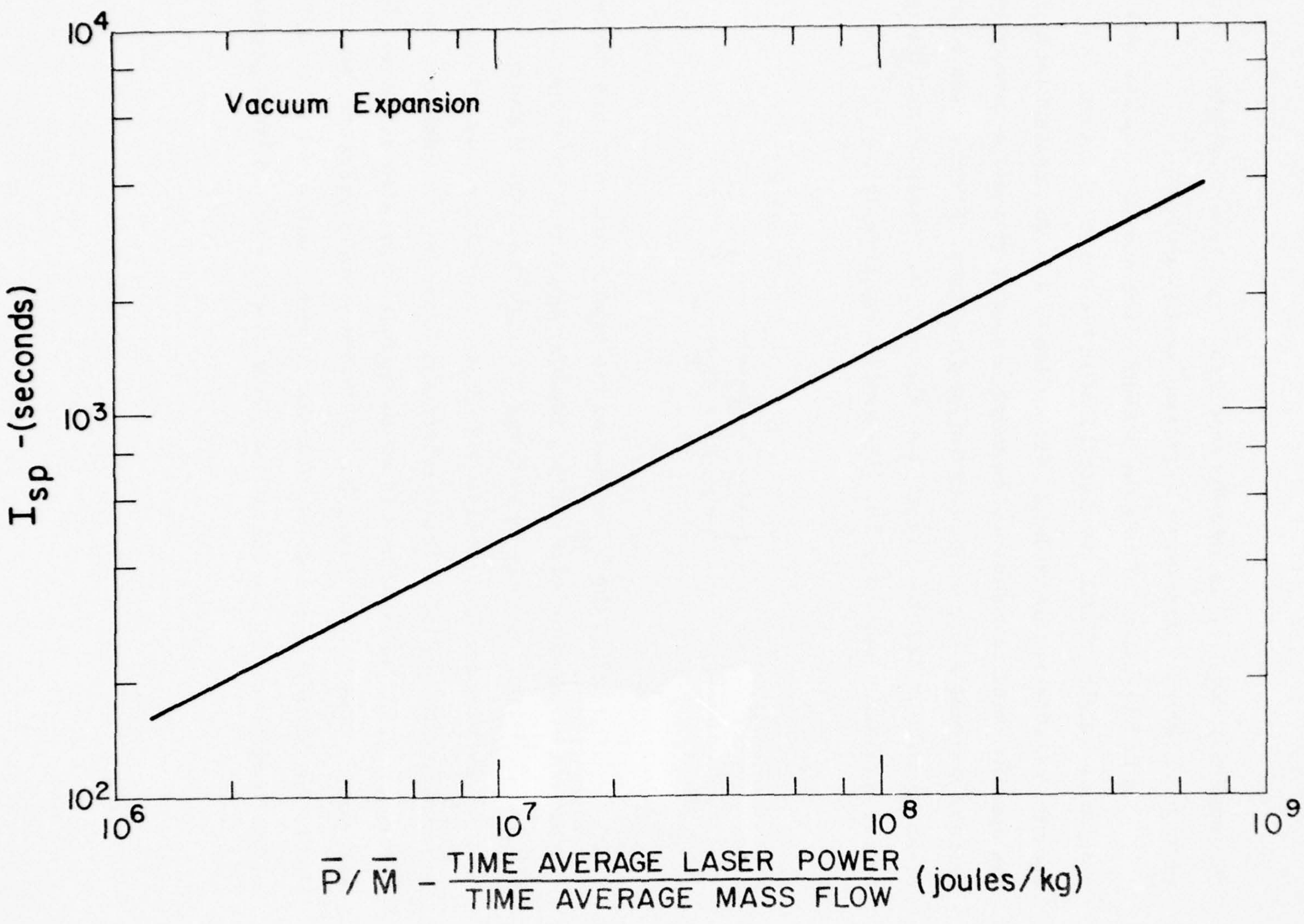

Fig. 8 Specific Impulse

Subsequently, Eq. (17) is actually a general expression evaluated for that value of e_R which corresponds to pulsed laser propulsion.

It is interesting to note the scaling of the specific impulse with molecular weight. First, we recall that in the chemical rocket, the specific impulse scales in direct proportion to u^*. At constant temperature, the specific impulse scales as the inverse square root of the molecular weight, thereby favoring a low molecular weight propellant. For the case of pulsed laser propulsion, we shall retain both the chamber pressure and the laser power constant. Rewriting Eq. (17) with ρ^* replaced by $\gamma\, p^*/(u^*)^2$, we obtain

$$I_{sp} = \frac{1.6}{g} \left(\frac{u^* E}{\gamma\, p^* (D^*)^2 (t_p - t_s)} \right)^{1/2} ,$$

which illustrates that the I_{sp} scales as the square root of u^* and the inverse fourth root of the molecular weight, thereby favoring a low molecular weight propellant, but only by as large a margin as in the chemical rocket.

The results illustrated in Fig. 8 are appropriate only for nozzles exhausting with negligible temperature and pressure. In addition, we have inherently assumed that there is no divergence of the flow at the nozzle exit plane. The loss in thrust due to a finite ambient pressure, and that due to the finite size and shape of rocket nozzles, will now be determined in order to demonstrate the operational limitations of pulsed laser propulsion.

V. OPERATIONAL LIMITATIONS

There are several effects which limit the specific impulse that we may obtain from a pulsed laser propulsion system such as that analyzed in the previous sections. They are:

1) Finite divergence of the nozzle

2) Finite length of the nozzle.

3) Finite ambient pressure.

These three effects can be included in the present fluid mechanical analysis of pulsed laser propulsion.

In determining the thrust from a pulsed laser propelled rocket, we have assumed, without explicitly stating, that the rocket nozzle is contoured such that the initial conical flow may exhaust from the nozzle without divergence. In the absence of any such contouring, some thrust will be lost due to the divergence of the flow. The effect is easily assessed by determining the mass average of $u_e \cos\theta$, rather than the mass average of u_e. The thrust is reduced by the factor

$$\frac{\sin^2 \theta_C}{2\,(1 - \cos\theta_C)}$$

where θ_C is the cone half angle and is related to Ω by

$$\Omega = 2\pi\,(1 - \cos\theta_C)\ .$$

Results are illustrated in Fig. 9. For cone half angles of 10°, 20° and 30°, the thrust is reduced by 1%, 3% and 7%, respectively. Hence, nozzle

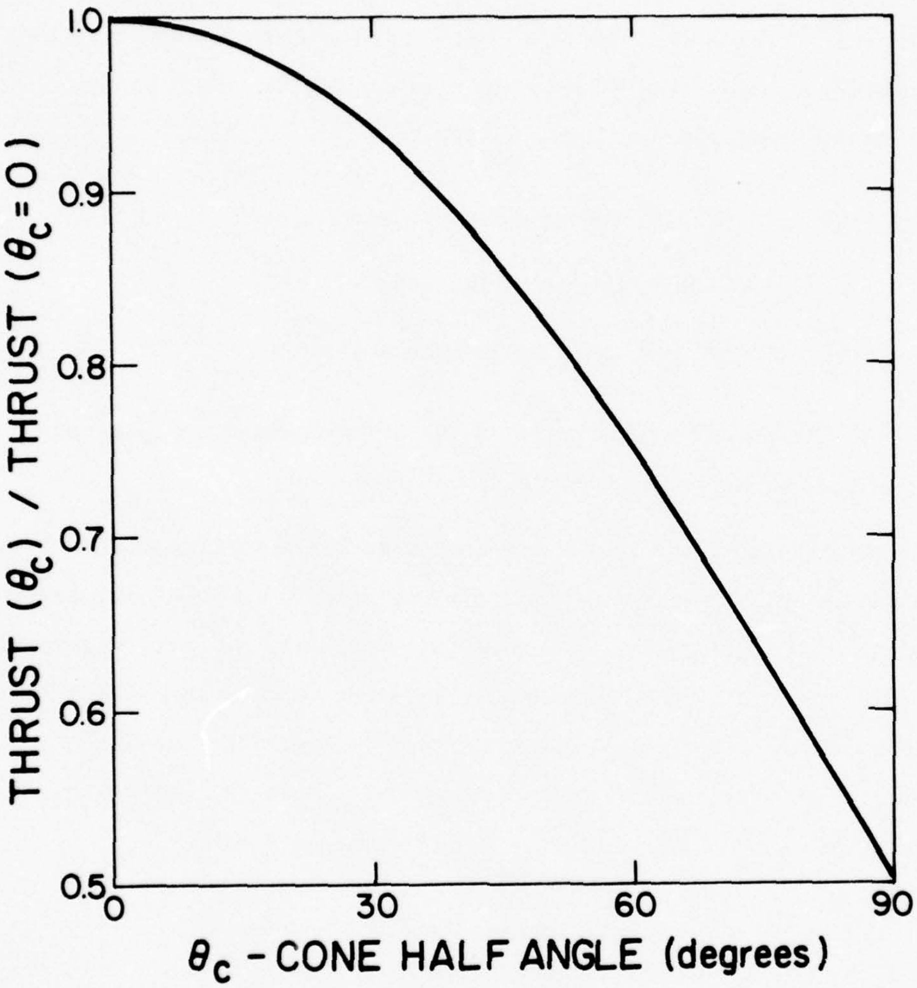

Fig. 9 Thrust Reduction Due to Flow Divergence

contouring will be a refinement, rather than a primary fluid mechanical consideration. A preliminary assessment of the effects of a continuously changing nozzle wall angle (eg. a parabolic nozzle) is presented in the Appendix.

The length of the nozzle is restricted by the radius of the shock at "break through". The shock must be contained within the nozzle, otherwise the specific impulse will be reduced. This is expressed as

$$L \geq R_s (t_b) \quad , \tag{18}$$

where L is the nozzle length and $R_s (t_b)$ is the shock "break through" radius, given by Eq. (13).

$$R_s (t_b) = \sqrt{\frac{\gamma + 1}{\gamma - 1}} \left(\frac{t_p - t_s}{D^* / u^*} \right) D^* \tag{19}$$

However, satisfying Eq. (18) does not insure that the maximum thrust is obtained from the energy deposition. In order to obtain the results quoted in Fig. 8, the gas must expand to a vacuum while still within the nozzle. To determine the effect of the finite value of L on the I_{sp}, we allow the gas to expand isentropically to the exit plane at r = L. We conserve mass, entropy and energy by

$$\rho_e u_e L^2 = \rho_b u_b \eta_b^2 R_s^2 (t_b) \quad , \tag{20}$$

$$p_b / \rho_b^\gamma = p_e / \rho_e^\gamma \quad , \tag{21}$$

and

$$C_p T_e + 1/2 \, u_e^2 = C_p T_b + 1/2 \, u_b^2 \quad , \tag{22}$$

respectively, where the subscripts b and e denote "break through" and exit plane conditions, respectively. Solving for u_e, we obtain

$$u_e = u_s(t_b) \sqrt{h^2(\eta_b) + \gamma\, Y(\eta_b)\, g(\eta_b)/f(\eta_b)} \quad , \tag{23}$$

where $Y(\eta_b)$ is a weak function of u_e and must be determined by iteration. Denoting the Nth iteration by $Y^{(N)}$, we obtain

$$Y^{(N)} = 1 - (\eta_b/\ell)^{2(\gamma-1)} \left(\frac{u_s\, h}{u_e^{(N-1)}} \right)^{\gamma-1} \quad ,$$

where

$$\ell = L/R_s(t_b) \quad ,$$

$$u_e^{(0)} = h(\eta_b)\, u_s(t_b) \quad ,$$

and $u_e^{(N)}$ is determined from $Y^{(N)}$ via Eq. (23) for $N \geq 1$.

The reduced thrust and specific impulse due to the finite nozzle length is obtained by using the corrected value of u_e in the integrand of I_2. Results are illustrated in Fig. 10. For $\gamma = 1.4$, termination of the nozzle at the break through radius would result in a recovery of only 68% of the thrust. However, 90% of the thrust is recovered in three break through radii. Nozzle lengths greater than three $R_s(t_b)$ yield a deminishing return in terms of thrust recovered. We shall use $L = 3R_s(t_b)$ as a design criterion.

The finite ambient pressure will also reduce the specific impulse of the laser powered rocket. To illustrate the magnitude of this effect,

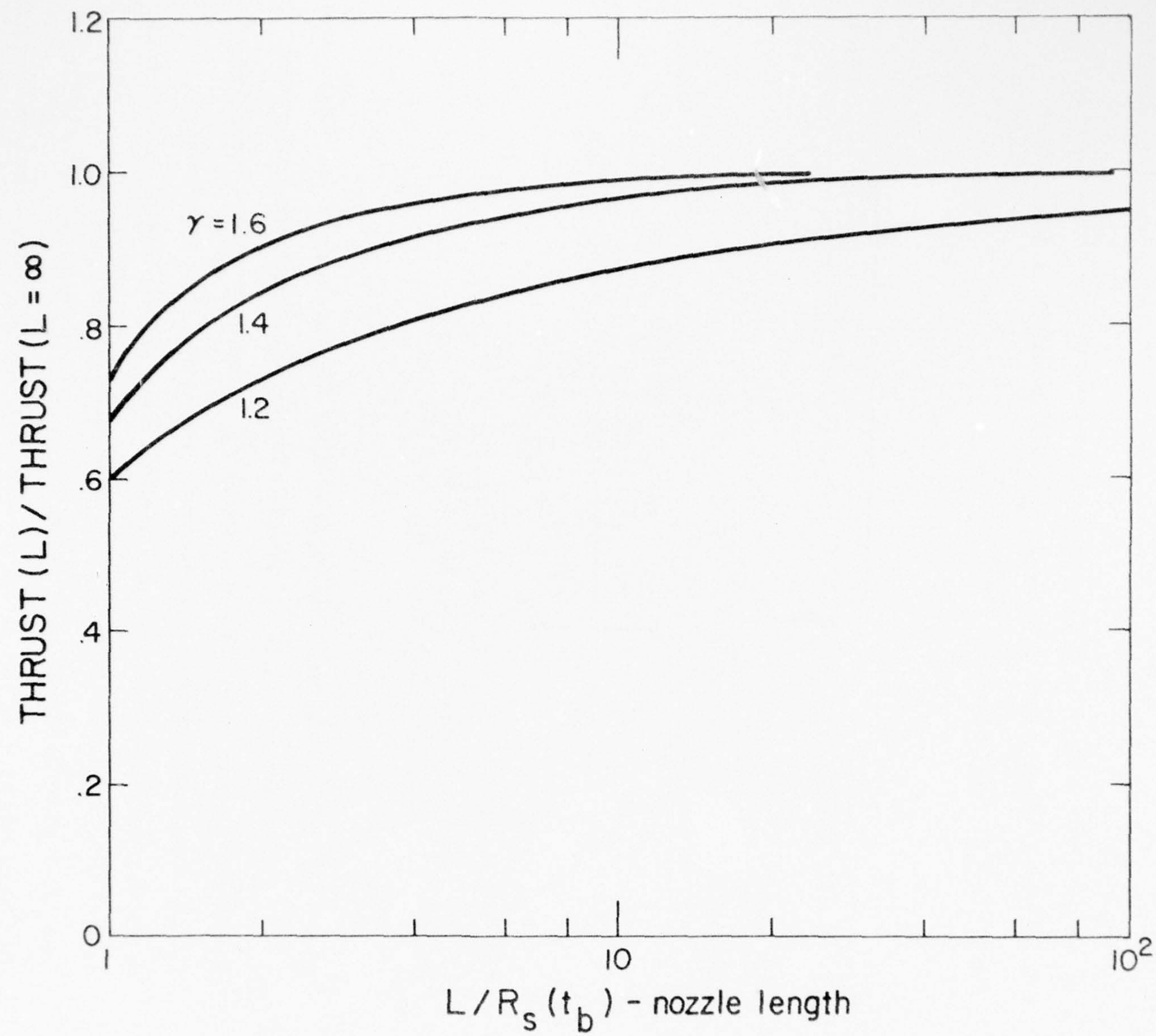

Fig. 10 Thrust Reduction Due to Finite Length Nozzles

we again allow the gas to expand isentropically from the "break through" conditions to the ambient pressure, p_∞. Conservation of energy and entropy, Eqs. (22) and (21), yield

$$u_e = u_s(t_b) \sqrt{h^2(\eta_b) + \gamma g(\eta_b)/f(\eta_b) - \Gamma(\eta_b)} \quad , \tag{24}$$

where

$$\Gamma(\eta_b) = \gamma \left[\frac{9(\gamma+1)^3}{8(\gamma-1)^2} I_1 Q_\infty \right]^{\frac{\gamma-1}{\gamma}} g^{\frac{1}{\gamma}}(\eta_b)/f(\eta_b) \quad ,$$

and

$$Q_\infty = \Omega p_\infty (u^*)^3 (t_p - t_s)^3 / E \quad ,$$

where Q_∞ is approximately the ratio of p_∞ to the pressure of the blast wave.

The reduced thrust and specific impulse due to the finite ambient pressure is obtained by using the corrected value of u_e in the integrand of I_2. Results are illustrated in Fig. 11. For a chamber pressure of two atmospheres (sufficient to "choke" the flow at sea level), the sonic pressure is one atm. Laser energies sufficient to create a $30{,}000^\circ K$ plasma would result in a blast wave pressure of 100 atm. Thus, the sea level value of Q_∞ would be 10^{-2} and, for $\gamma = 1.4$, 75% of the vacuum thrust would be obtained. Raising the chamber pressure to 20 atm would result in a 1000 atmosphere blast wave and a recovery of 90% of the vacuum thrust. Higher chamber pressures yield

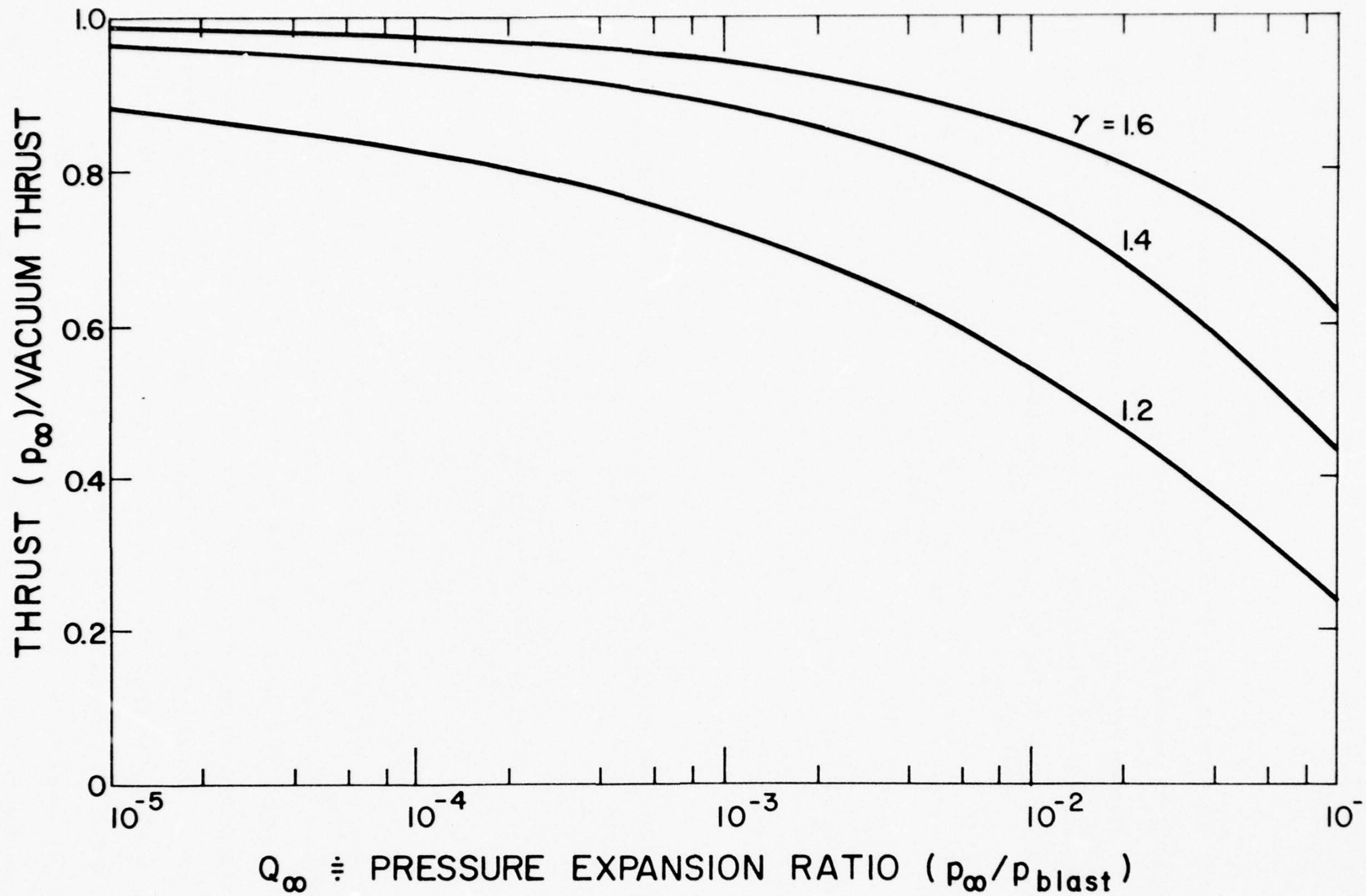

Fig. 11 Thrust Reduction Due to Finite Ambient Pressure

diminishing returns in the thrust recovered and would begin to introduce thermodynamic and structural penalties.

Having determined the limitations for which the results of Sec. IV are valid, we will illustrate the results by way of a simple example. From Sec. III, we recall the relation between power $\overline{P}$ and thrust $\overline{T}$

$$\overline{P} = g\, I_{sp}\, \overline{T}/2 \quad , \tag{25}$$

where $e_R \equiv 1$ and

$$\overline{P} = E/t_p \quad . \tag{26}$$

Equations (17) and (25) yield the size of a rocket required for the thrust $\overline{T}$.

$$D^* = \left(\frac{1.6}{g\, I_{sp}}\right) \left(\frac{g\, I_{sp}}{2\rho^* u^*}\right)^{1/2} \left(\frac{t_p}{t_p - t_s}\right)^{1/2} \left(\overline{T}\right)^{1/2} \tag{27}$$

If we wish to design a rocket to operate with a chamber pressure of two atmospheres and temperature of $300^{\circ}K$, the sonic density and velocity become 10^{-3} gm/cc and 30,000 cm/sec, respectively. With a specific impulse of 800 seconds, we may consider launching a one ton rocket with 10 g's acceleration. This requires an orifice diameter of 22 cm and a power of 350 megawatts, as indicated in Figs. 12 and 13, respectively. In a laboratory experiment (to be discussed in Sec. VII) we may consider an equivalent acceleration of a 2 pound rocket which requires $D^* = 7$ mm and $\overline{P} = .35$ megawatts, also indicated in Figs. 12 and 13 respectively. The remaining point to emphasize is that there are distinct combinations of E and t_p permitted by the nozzle fluid mechanics. These are illustrated in Fig. 14.

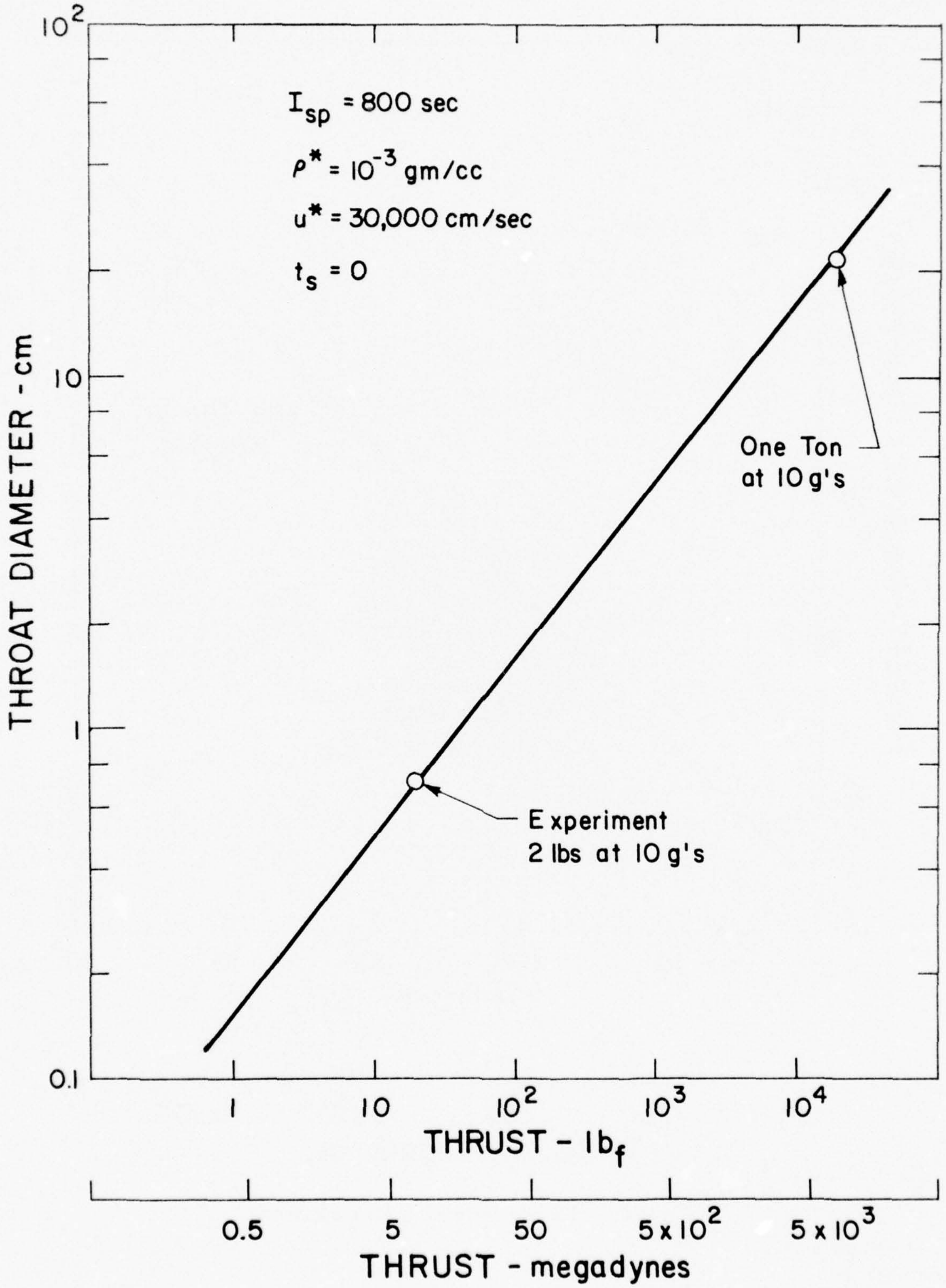

Fig. 12 Rocket Size Requirements

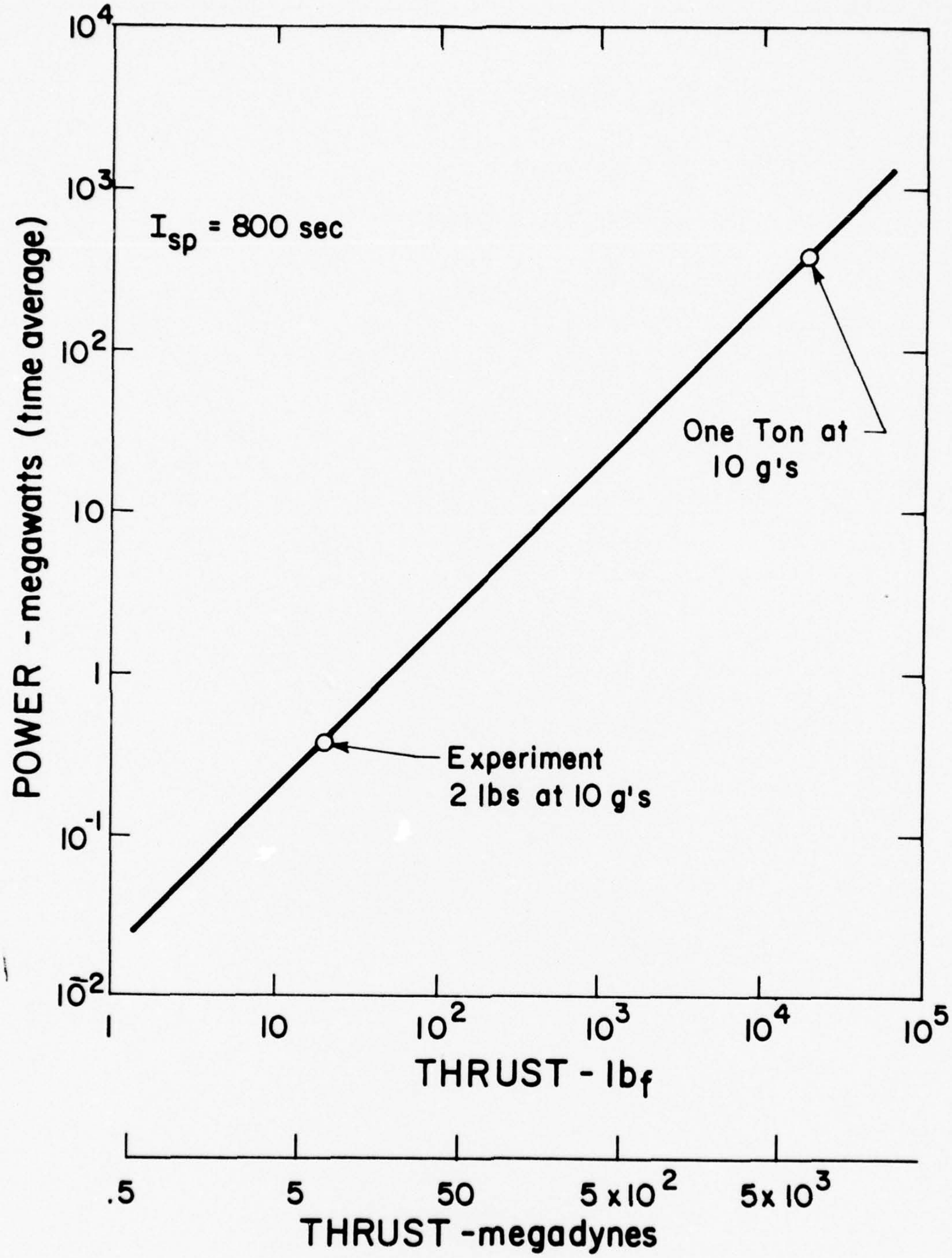

Fig. 13 Laser Power Requirements

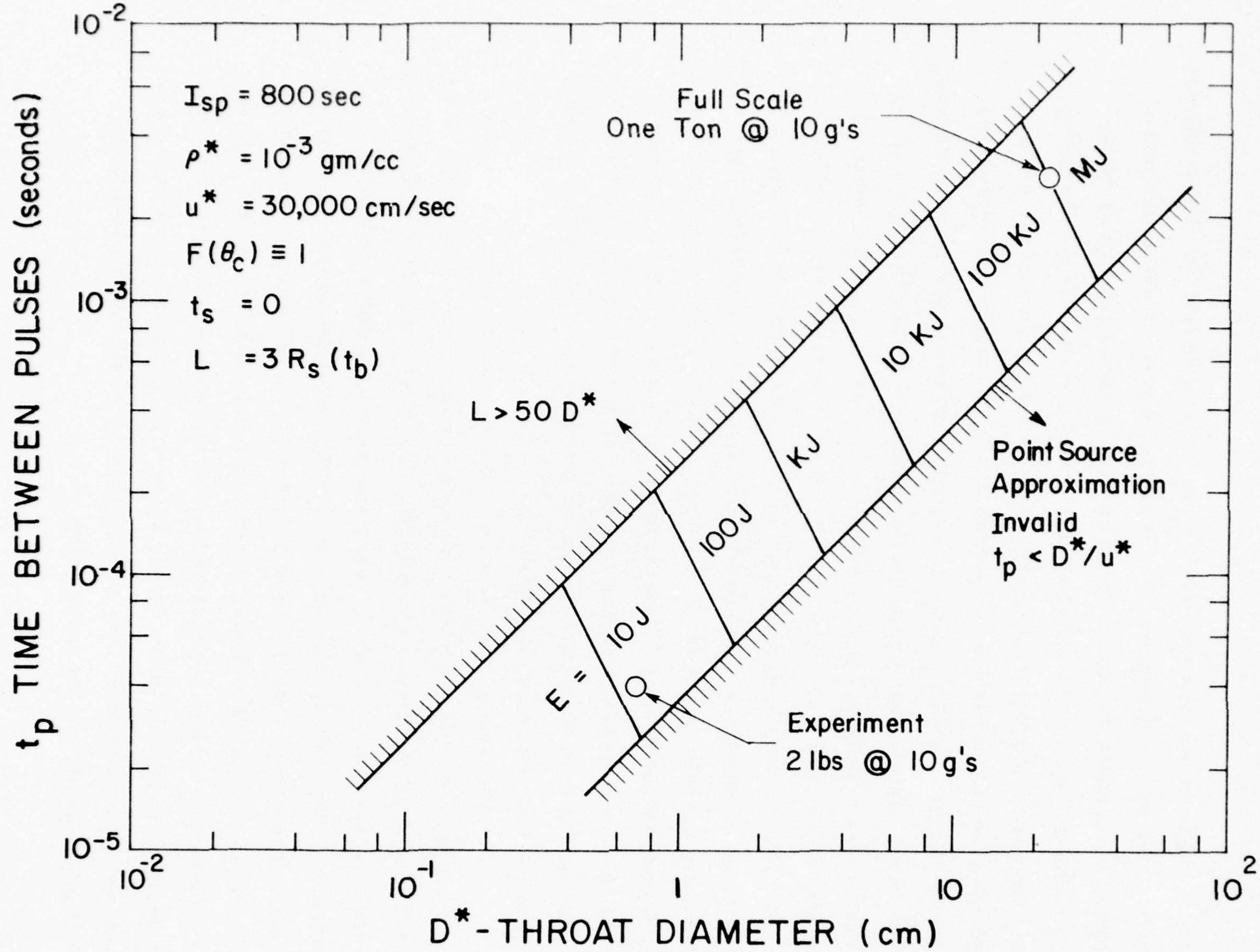

Fig. 14 Laser Energy Requirements

where we illustrate, from Eq. (17), t_p vs D^* at constant E. For arbitrary values of the orifice diameter, D^*, there is an upper limit on the pulse repetition frequency for which the point source approximation is valid. This reflects the fact that a finite time is required for the source gas to enter the rocket nozzle. There also exists a lower limit on the pulse repetition frequency for which a nozzle of a given length can recover the optimum thrust from the energy deposited. Larger time durations between pulses would permit the source gas to escape the nozzle before all of the pressure were converted to momentum. Our design criterion required that the nozzle length be three "break through" radii to recover 90% of the thrust. Nozzle lengths greater than 50 D^* are excluded on the basis of their large aspect ratio. The illustrative examples indicate that the laboratory experiment could be conducted with a 15 joule laser operating at 25,000 pulses per second. Launching one ton with 20,000 lb_f of thrust would require a megajoule laser operating at 350 pulses per second. The conditions for both the laboratory experiment and the "full scale" rocket are well within the realm of possibility.

Finally, using Figs. 12 - 14, we can determine the combination of laser energy and pulse repetition frequency (and therefore, average laser power) required to obtain a specific impulse of 800 sec. with a pulsed laser propulsion system. In Fig. 15 laser energy versus pulse repetition frequency (PRF), along with lines of constant average power (equal to E/t_p), is presented. The I_s = 800 sec. design curve, obtained from Figs. 12 - 14, is shown. In addition, a recommended laser pulse time for the specified laser energy is presented on the right hand ordinate. This scale is obtained using blast-wave theory along with the requirement that the blast wave does not propagate greater than one-half the throat diameter during the duration of the laser pulse.

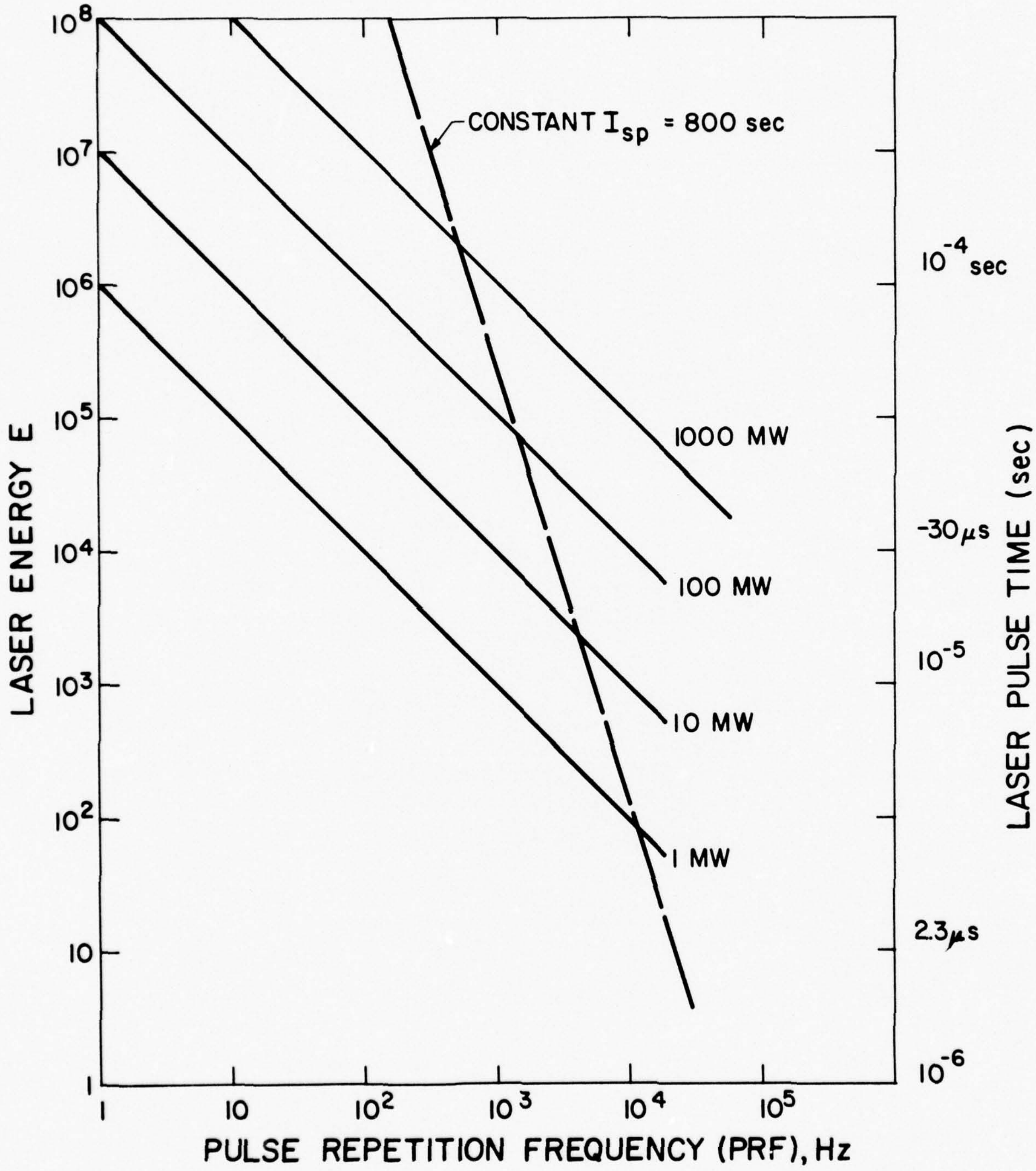

Fig. 15 Laser Energy vs. Pulse Repetition Frequency

VI. NOZZLE AND PLENUM PRESSURE TRACES

Practical engineering considerations make it necessary to illustrate the pressure distribution in the nozzle and plenum chamber (from which the propellant is supplied) as a function of space and time. The pressure behind the blast wave is given in Sec. II.

$$p_s\,(t) = \left(\frac{2}{\gamma + 1}\right)$$

Using Eqs. (1) and (4) we obtain

$$p_s = \frac{\left(\frac{8}{\gamma + 1}\right)\left(\frac{\gamma - 1}{\gamma + 1}\right)^{1/2} E}{9\,\Omega\, I_1\, R_s^{\,3}} \;,$$

which is illustrated in Fig. 16. For E = one megajoule, $\gamma = 1.4$ and $\Omega = 1$, the peak pressure is about 10^3 atm at the throat, decreasing to below one atm at L = 3 m.

The time history of the pressure at the throat is determined from $p_s\,(t)$ and $g\,(0)$, obtained from Fig. 3.

$$p\,(0,\ t) = \frac{\left(\frac{8}{\gamma + 1}\right)\left(\frac{\gamma - 1}{\gamma + 1}\right)^{1/2} \rho^{*}\,(D^{*})^{2}\ g\,(0)}{9\,t^{2}}$$

This pressure time history is illustrated in Fig. 17 for the one ton rocket. The throat pressure relaxes to below p^{*} in 10^{-4} seconds, which is small with respect to D^{*}/u^{*}. Therefore, the "source" restarts and establishes a

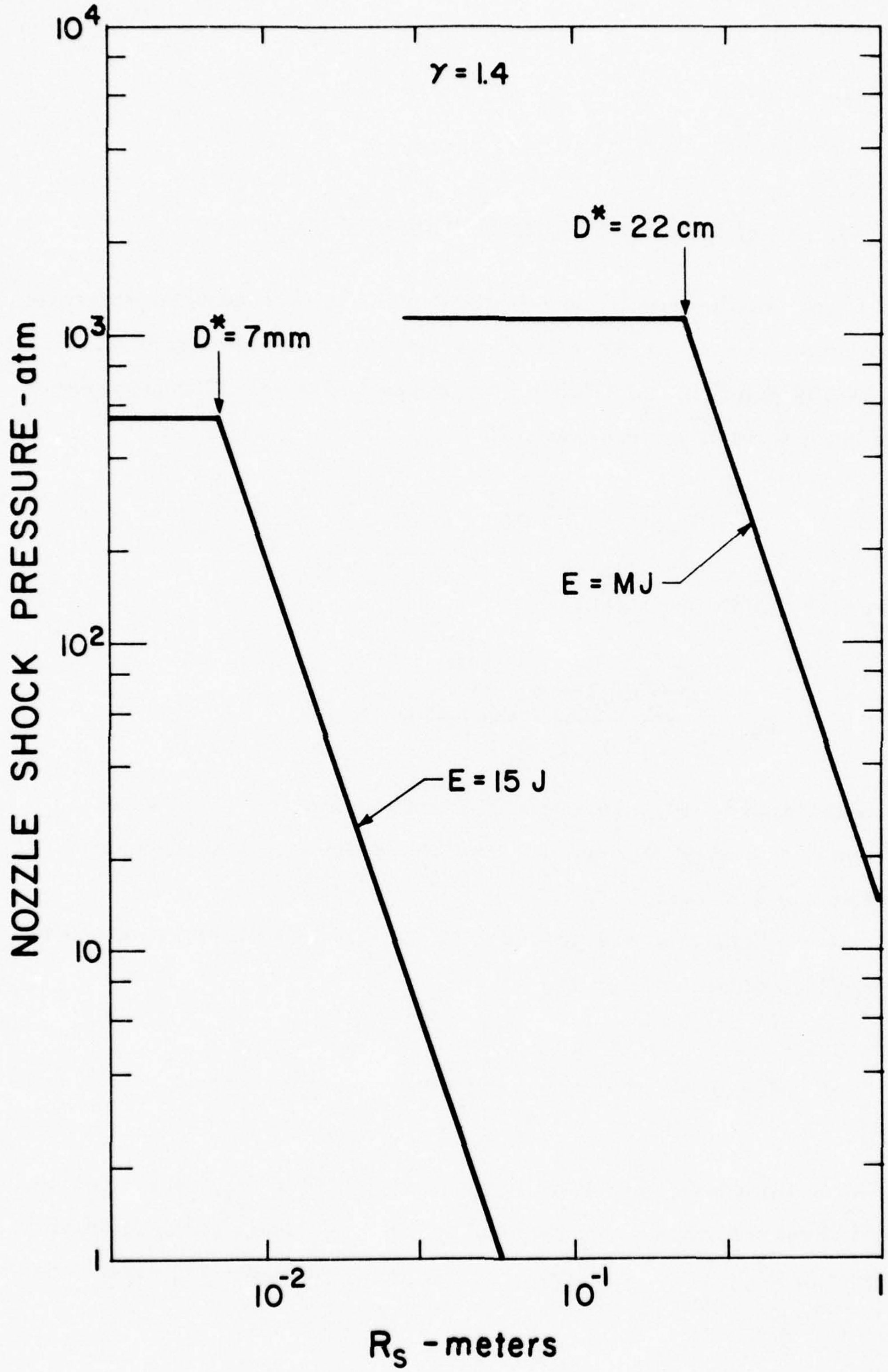

Fig. 16 Pressure Behind Nozzle Shock

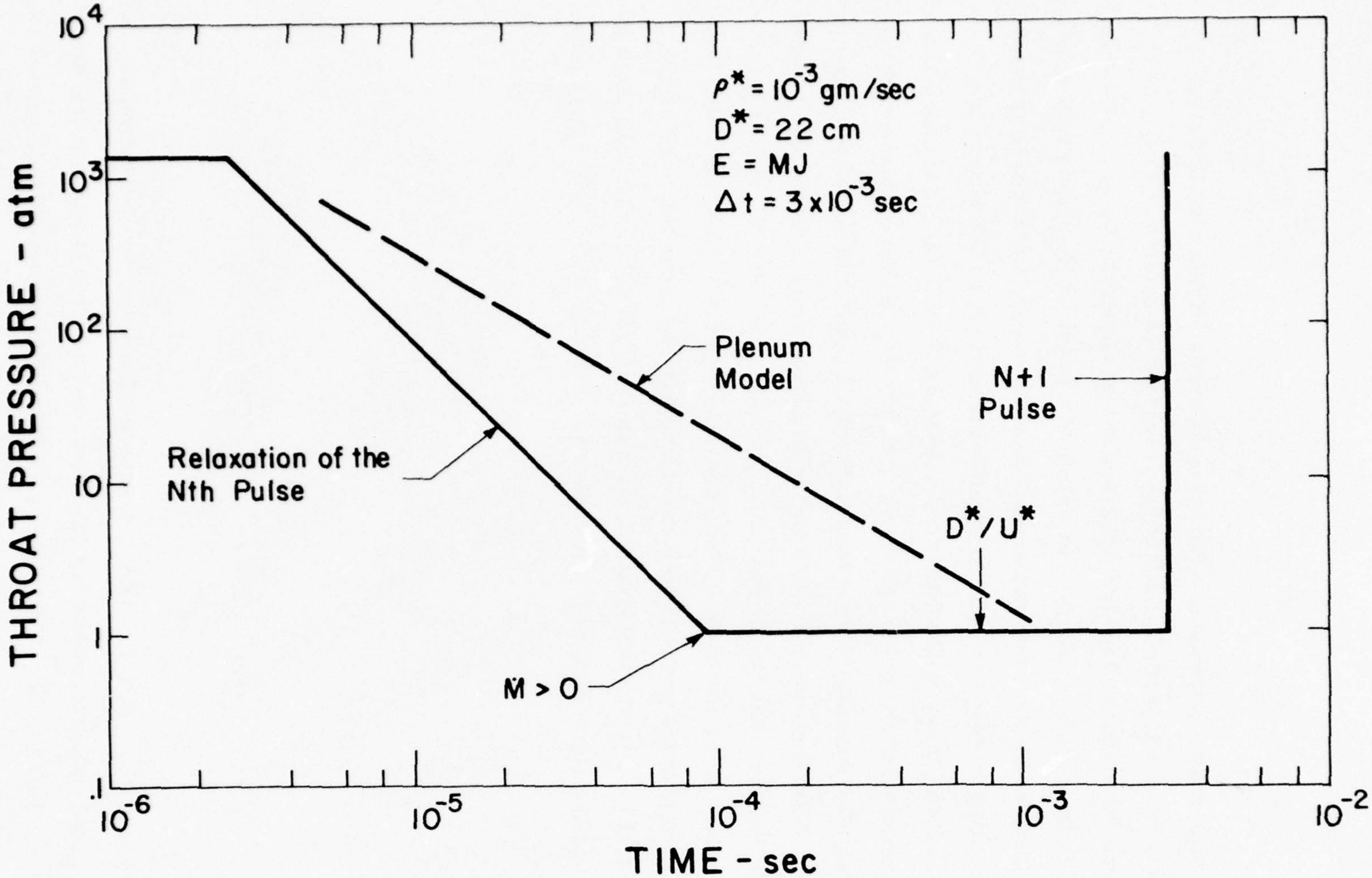

Fig. 17 Pressure Time History in Throat

new nozzle flow before the next pulse initiates another blast wave. The results quoted in Fig. 17 should be treated with caution. They are the results for an instantaneous point source of energy. We are using these results in spatial locations that are of the order of the deposition zone, and therefore some error is expected. Furthermore, and most important, we are quoting times that may be small with respect to the energy deposition time. If the laser pulse duration is greater than 2 microseconds, the early time portion of the pressure pulse is in error. At times large with respect to the pulse duration time, the point source approximation becomes valid.

A further complication in the pressure time history at the throat is due to the fact that the throat diameter is finite. Hence, the blast not only propagates down the nozzle, but into the plenum chamber as well. This high pressure plenum gas will also create deviations from the predictions made in Fig. 17. Suppose we model the plenum shock as a spherical blast wave propagating into a uniform atmosphere. Conventional blast wave theory yields

$$R_{s_1} = \zeta_o \left(\frac{E}{\rho_o}\right)^{1/5} t^{2/5}$$

and

$$p_{s_1} = \left(\frac{4}{25}\right) \zeta_o^{\,2} \left(\frac{2}{\gamma + 1}\right) \rho_o \left(\frac{E}{\rho_o}\right)^{2/5} t^{-6/5} ,$$

where $\zeta_o = \zeta_o(\gamma) \approx 1$. The pressure at the throat is approximately one half of p_{s_1} and this approximation for the pressure time history at the throat is also indicated in Fig. 17. The plenum model yields a much higher pressure which indicates that the mass flux begins earlier than 10^{-4} seconds but the pressure

does not relax to p^* until 10^{-3} seconds. This is, however, still well in advance of the next pulse. The location of the plenum shock at the time of pressure relaxation is also obtained from the spherical blast wave model and corresponds to one meter at 10^{-3} seconds. This length scale is in excess of the throat diameter (22 cm) and may be as large as the plenum chamber itself. This creates two potential problems. First: each pulse will be detonated in a gas which has already been processed by the plenum shock and secondly, the mechanical pumps supplying the expellant to the plenum chamber may have to work against a higher back pressure. An assessment of these effects and any correction thereof is beyond the scope of this study.

VII. EXPERIMENT DESIGN

An experiment designed to test the pulsed laser propulsion concept can be performed using pulsed CO_2 TEA lasers. The objectives of such an experiment are to (1) verify the theoretical predictions of high specific impulse with relative efficiency near unity, (2) examine the dependence of the time averaged specific impulse and thrust upon average laser power and repetition rate, (3) study the effects of finite exit plane pressure upon thrust and specific impulse and (4) determine how the effects of energy lost to the walls along with the finite source nature of the breakdown process will affect rocket performance and comparison with theory.

Multiple independently triggered pulsed CO_2 TEA lasers can be utilized for such experiments. The pulse shape of such a laser is typically composed of a 100 nsec spike with a one to three μsec tail. The tail of the pulse can be virtually eliminated by reducing the amount of nitrogen in the active medium. Therefore, the effects of the tail of the pulse on the rocket performance can be examined. A "fifteen joule" CO_2 TEA laser will deliver 5 J within a 100 nsec laser pulse, or 15 J within a 100 nsec spike and a 3 μsec tail. The minimum number of lasers required to achieve complete simulation of multiple pulse performance is not clear. However, at least two pulses are necessary to determine if the independence of each pulse, assumed theoretically, is realistic. A schematic of an experiment, which utilizes four lasers of 15 J each, is presented in Fig. 18. The four laser beams will be directed into the vacuum chamber through a window at slightly different angles of incidence (up to 10^{-2} radians apart) so the focused spots will be on the order of a centimeter in diameter. Therefore, the performance should be equivalent to that obtained with co-linear laser beams. The lasers are individually triggered, and thus, various interpulse

PRECEDING PAGE BLANK-NOT FILMED

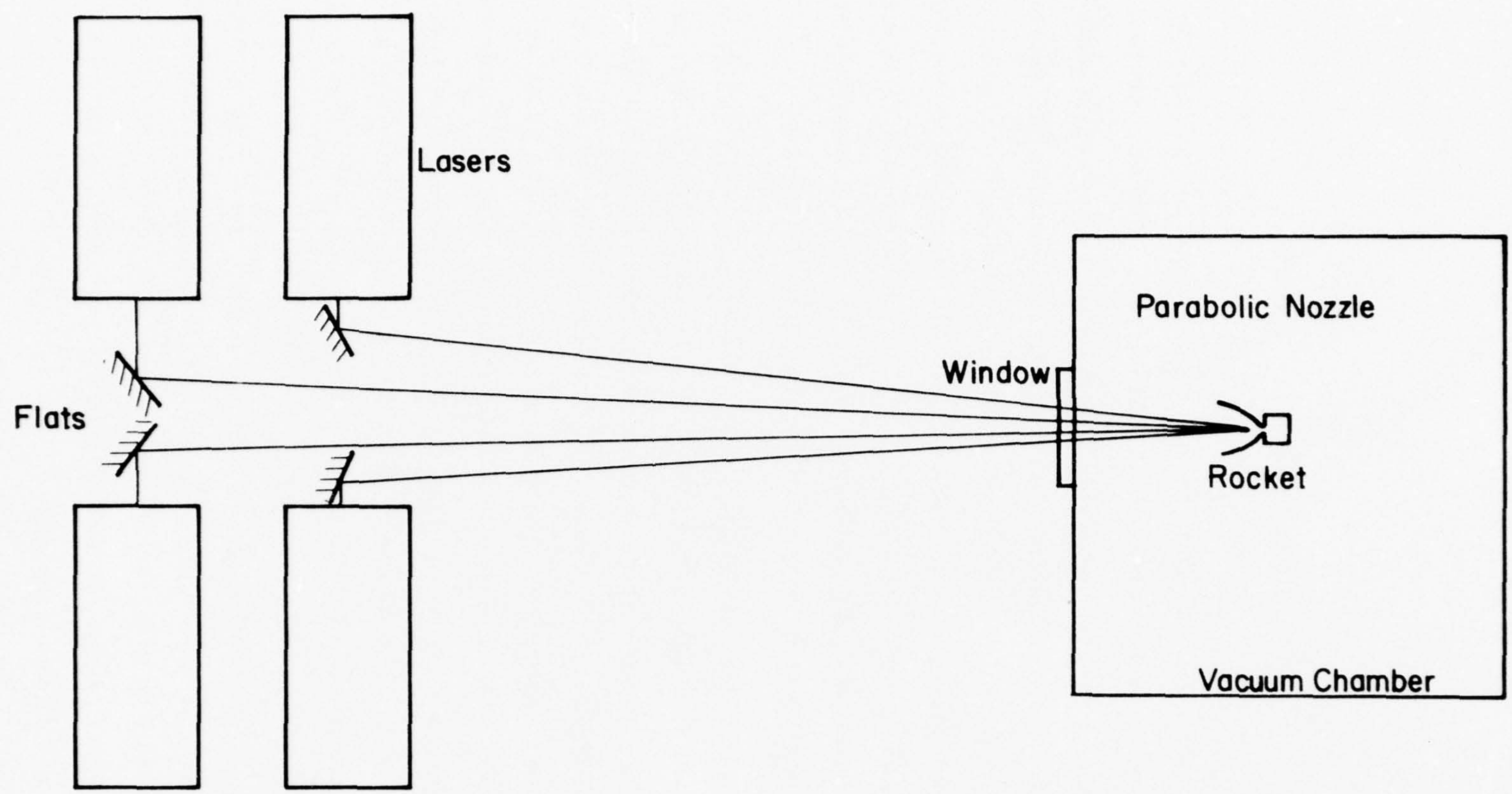

Fig. 18 Pulsed Laser Propulsion Experiment Schematic with Parabolic Nozzle

times can be programmed to obtain the desired pulse repetition rates. At a repetition rate of 10,000 pps, this laser system will deliver an average laser power of 150 kilowatts. The size of the rocket nozzle and the anticipated performance of such a system will be determined from theoretical predictions, and will be discussed later.

Diagnostics

The thrust and specific impulse are the two parameters which will characterize the performance of the pulsed laser propulsion system. The relationship between thrust, average power and specific impulse is given by Eq. (25), and the average power as a function of laser energy and repetition rate is given by Eq. (26). The thrust anticipated from the four 15 J laser pulse system as a function of specific impulse and repetition rate is presented in Fig. 19. The thrust can be measured either by using a load cell to obtain the instantaneous thrust or by using a ballistic pendulum to measure the delivered total impulse/pulse and dividing it by the time between pulses to determine the time averaged thrust. The ballistic pendulum is a simple device which directly measures the total delivered impulse. However, since the pendulum must be free to swing, the propellant must be carried as an integral part of the pendulum structure. The load cell provides instantaneous thrust, but the inherent response time of the cell and its response to acoustic ringing in the nozzle wall may make qualitative results difficult. It is most desirable to use the load cell combined with nozzle wall pressure transducers (as in Ref. 4) to deduce the pressure/time history along with the thrust/time history. Comparison with integrated thrust (or impulse) from a ballistic pendulum will serve as a calibration of the load cell response.

The specific impulse is difficult to measure directly. It can be obtained if the impulse and the amount of gas expelled from the nozzles is measurable. A more promising approach to determining specific impulse

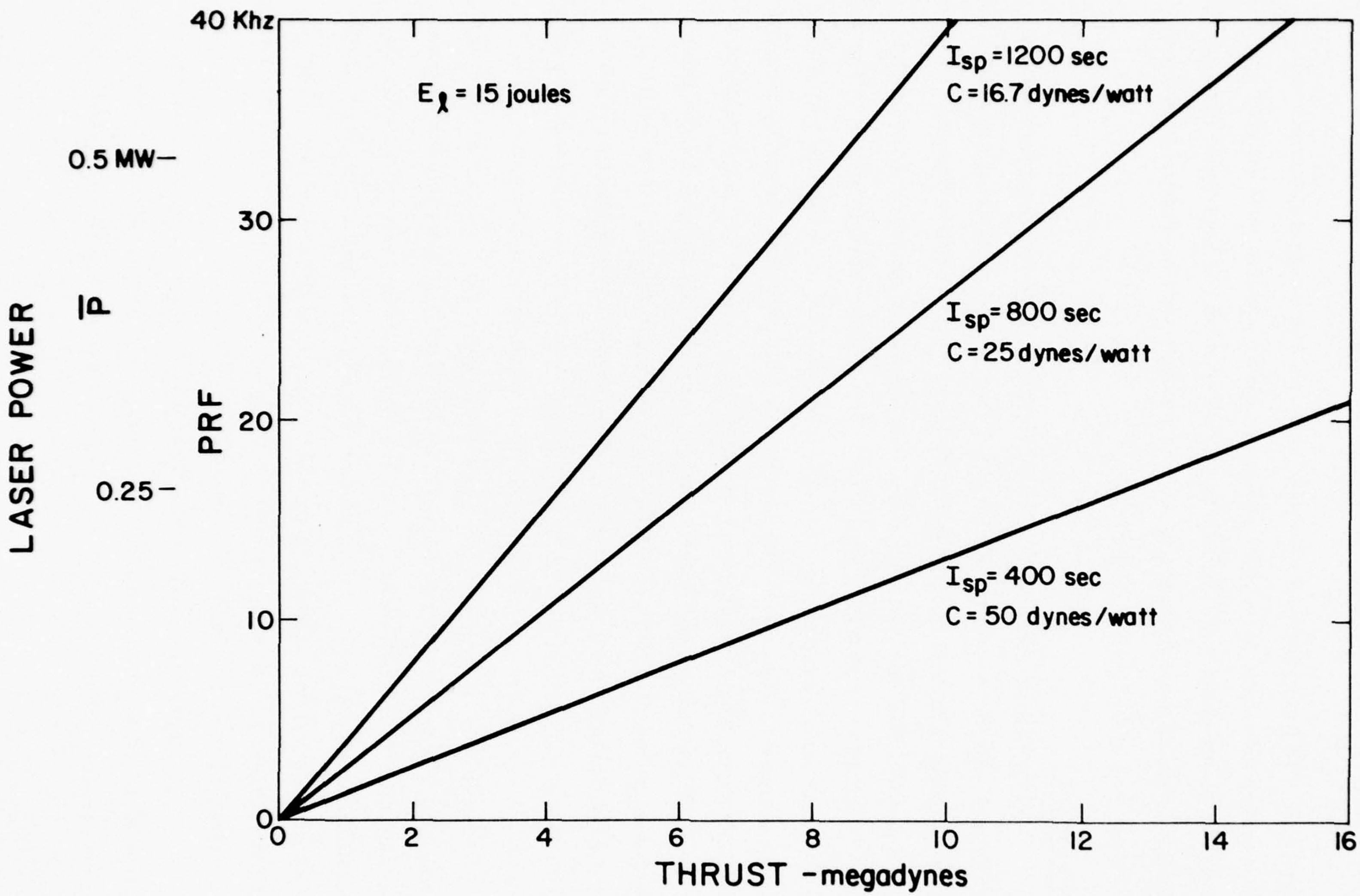

Fig. 19 Laser Power and Pulse Repetition Rate vs. Rocket Thrust

is to directly measure the exhaust velocity. The technique that will be used involves multiple sparks in the flow field from the same set of electrodes.[15] The hot, partially ionized gas flows with the instantaneous exhaust velocity. Therefore, after one spark is ignited, the hot gas propagates at the exhaust velocity. A second spark is then ignited at the new position of the partially ionized gas. By measuring the distance between the first and second spark positions, the exhaust velocity is determined (see Fig. 20 and Ref. 15). For CW measurements with a streak or framing camera, a version of Jacob's ladder could be made. The familiar Jacob's ladder spark rises because of free convection, while in the present case the spark convects downstream at the exhaust velocity. A streak camera measurement yields information along a specified section of the flow field while a framing camera is used to obtain velocity as a function of distance from the nozzle centerline. However, neither of these techniques will result in the velocity at the exhaust plane as a function of time.

Nozzle Design and Propellant Supply Considerations

It is desirable to perform experiments in pulsed laser propulsion using two distinct nozzle configurations. Since theoretical modeling has been completed for a conical nozzle, it is essential to perform a series of experiments with such a nozzle to verify the theoretical predictions. This configuration is gasdynamically the simplest, and beam focusing is accomplished externally which permits control and variation of spot size and breakdown location. On the other hand since an actual system may utilize a self-focusing nozzle, experiments with a parabolic nozzle should also be performed. This nozzle is optically optimum and permits near spherical focusing of a collimated laser beam. Experiments with this nozzle shape are necessary to assess any aerodynamic penalties resulting from wall curvature (due to the unsteady nature of the flow as discussed in the Appendix) and determine the effectiveness of the self focusing concept

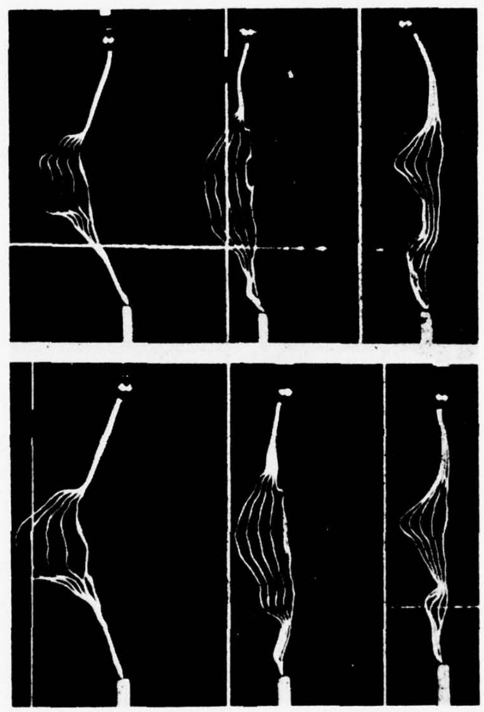

Fig. 20 Example of Spark Technique for Measuring Exhaust Velocity from Ref. 15

to obtain a strong laser induced breakdown at the focal point. Nozzle sizing is accomplished by using the theoretical predictions for optimum performance. Essential experiments to be performed are as follows:

1. Using a conical nozzle in a vacuum chamber with an external propellant source, perform a series of experiments to determine the specific impulse as a function of average laser power/mass flow (Fig. 8). In addition, it is desirable to explore the operating corridor in repetition rate at constant specific impulse (e.g. Fig. 14, where $I_{sp} = 800$ sec).
2. Using the conical nozzle at a specific design point, examine the effect of finite exhaust plane pressure on the observed thrust and specific impulse.
3. The above experiments with two, three and four laser pulses should be performed to determine the independence of each thrusting sequence along with the pressure/time history in the propellant plenum chamber.
4. A selected number of the above experiments with a parabolic nozzle should be performed to determine the focusing ability of the nozzle and the aerodynamic penalties of the wall curvature.

When sizing the nozzle for vacuum experiments, we want to be sure the nozzle is sufficiently long for the experiments which are to be performed at various repetition rates. Theoretically, we have determined that it is desirable to have the nozzle length equal to at least $3 R_b$ where R_b is the "breakthrough" radius. Equation (19) relates this radius to the time between laser pulses and the sonic velocity of the propellant at the entrance to the nozzle. If the plenum is at room temperature and $\gamma = 1.4$, $u^* \approx 3.22 \times 10^4$ cm/sec., and from Eq. (19)

$$R_b (t_p) \cong 8 \times 10^4 (t_p - t_s).$$

For lasers of 5 to 15 J it is desirable to operate in a repetition rate regime such that $10^{-5} < t_p - t_s < 10^{-4}$. Since in a vacuum there is no penalty for having the nozzle too long, it is best to design around $(t_p - t_s) = 10^{-4}$. Therefore $R_b(t_p) \cong 8$ cm. and a recommended nozzle length would be $L = 24$ cm. Since it is desirable to "choke" the propellant flow at sea level for earth-based missions we shall calculate the plenum chamber conditions for an experiment based upon $p^* = 1$ atm. The resulting stagnation pressure for $\gamma = 1.4$ becomes $p_o = 1.9$ atm and with a plenum temperature $T_o = 300^oK$, we obtain $\rho_o = 2.13 \times 10^{-3}$ gms/cm^3 and $\rho^* = 1.35 \times 10^{-3}$ gms/cm^3. In order to determine the propellant mass flow rate it is necessary to choose a throat diameter. The best way to operate in the corridor of Fig. 14 is fix the throat diameter and vary the laser energy and the time between pulses. For laser energies between 5 and 15 J a throat diameter $D^* = 0.5$ cm. will permit operation at $I_{sp} = 800$ sec. when the time between laser pulses is $2 \times 10^{-5} < t_p - t_s < 10^{-4}$ sec. If $D^* = 0.5$ cm., $A^* \cong .2$ cm^2 and the mass flow rate equals 8.5 gms/sec. The volume of the propellant supply chamber (or plenum) required to perform an experiment with four laser pulses, for example, can now be calculated. If the lasers are pulsed at the slowest repetition rate of 10^4 pps and the laser pulse time is 2 μsec, the entire experiment is completed in approximately 4×10^{-4} sec. At a propellant mass flow of 8.5 gms/sec. this corresponds to a total propellant mass utilized $M \cong 3.5 \times 10^{-3}$ gms. If $\rho_o = 2.13 \times 10^{-3}$ gms/cm^3, the volume of propellant utilized $\Delta V \cong 1.6$ cm^3. It is desirable to have the change in propellant volume not exceed 10% of the total propellant volume. Therefore, a plenum of 16 cm^3 is desired.

A schematic of the above nozzle designed for experiments with four pulsed TEA lasers of 5 to 15 J is shown in Fig. 21. Since the unit should be completely self contained for operation in a vacuum chamber, the

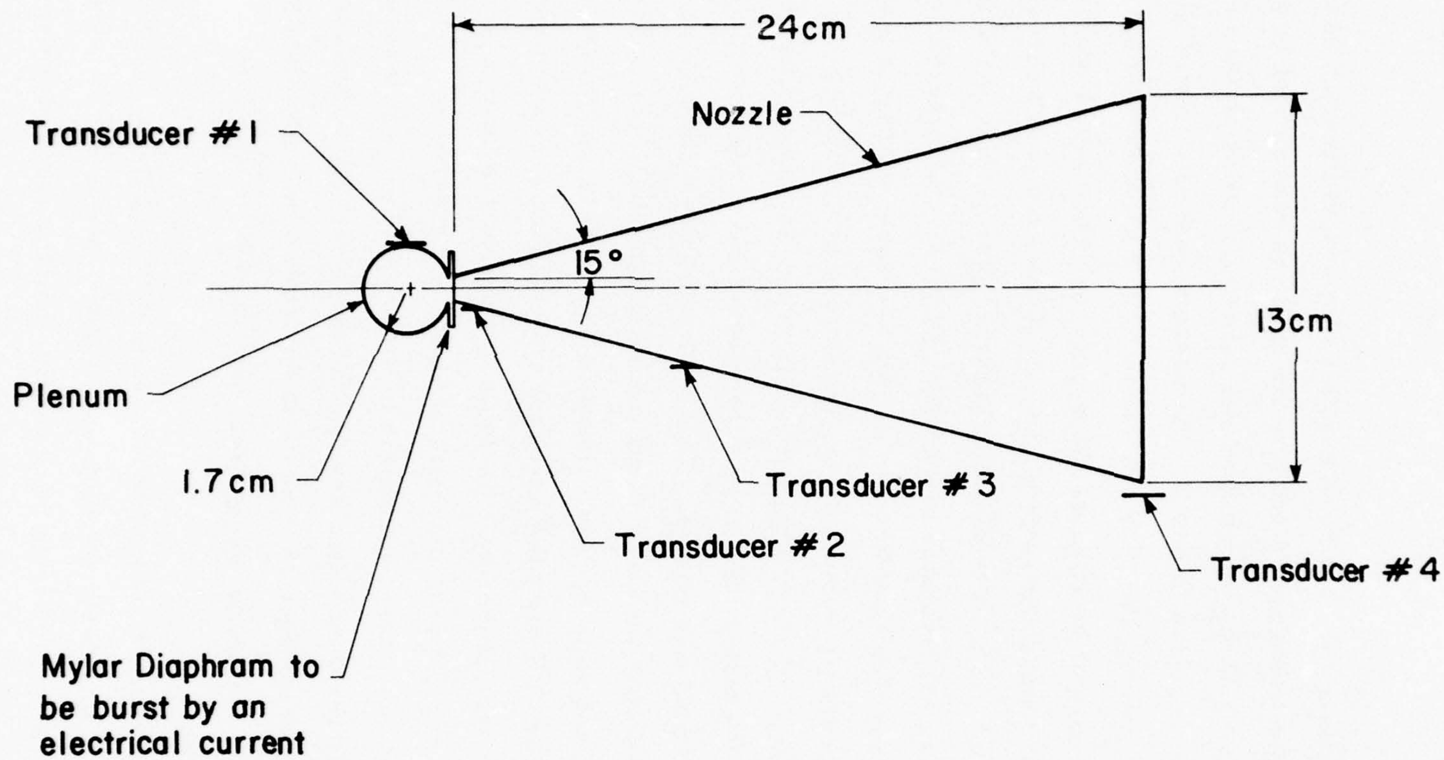

Fig. 21 Conical Nozzle Design

plenum is attached to the nozzle with a diaphragm inserted to maintain the stagnation pressure in the plenum until the experiment is performed. Precise timing of the bursting of the diaphragm prior to the laser pulse is desirable in order to prevent the vacuum chamber from filling up with propellant, raising the chamber pressure. With a supersonic propellant flow in the nozzle the exhaust plane pressure should be maintained at 2×10^{-2} torr since the ratio of the exit plane area to the throat area is approximately 700. Use of a diaphragmed plenum may make turn-around time between experiments longer than desired, but experiments with a steady source of propellant into the nozzle would require a large pumping capacity if experiments are to be performed in a vacuum.

In Fig. 21 the nozzle half angle has been taken to be 15°. Thus, from Fig. 9 greater than 95% of the theoretical thrust estimate can be anticipated with this nozzle. This angle also does not impose severe restrictions upon the beam focusing requirements which are discussed in the next subsection. Also shown in Fig. 21 are the suggested optimum locations for wall mounted pressure transducers. Transducer No. 1 is mounted in the plenum wall in order to monitor the change in the stagnation pressure over the four thrusting pulses. Transducer No. 2 is mounted as close to the throat as possible in order to obtain a measurement of the pressure in the breakdown region. Transducer No. 3 is placed at the estimated "breakthrough" radius to determine the propellant pressure prior to the isentropic expansion, and transducer No. 4 is mounted in the exhaust plane.

A schematic of a parabolic nozzle arrangement is shown in Fig. 22 This nozzle was designed such that A_e/A^*, where A_e is the exit plane area, is the same as the cone nozzle, and the angle at which the flow leaves the nozzle is 15°, as it is with the cone nozzle. The corresponding length, however, is now only 1.5 "breakthrough" radii. The overall effect of the shortened length and parabolic shape of the nozzle must be assessed

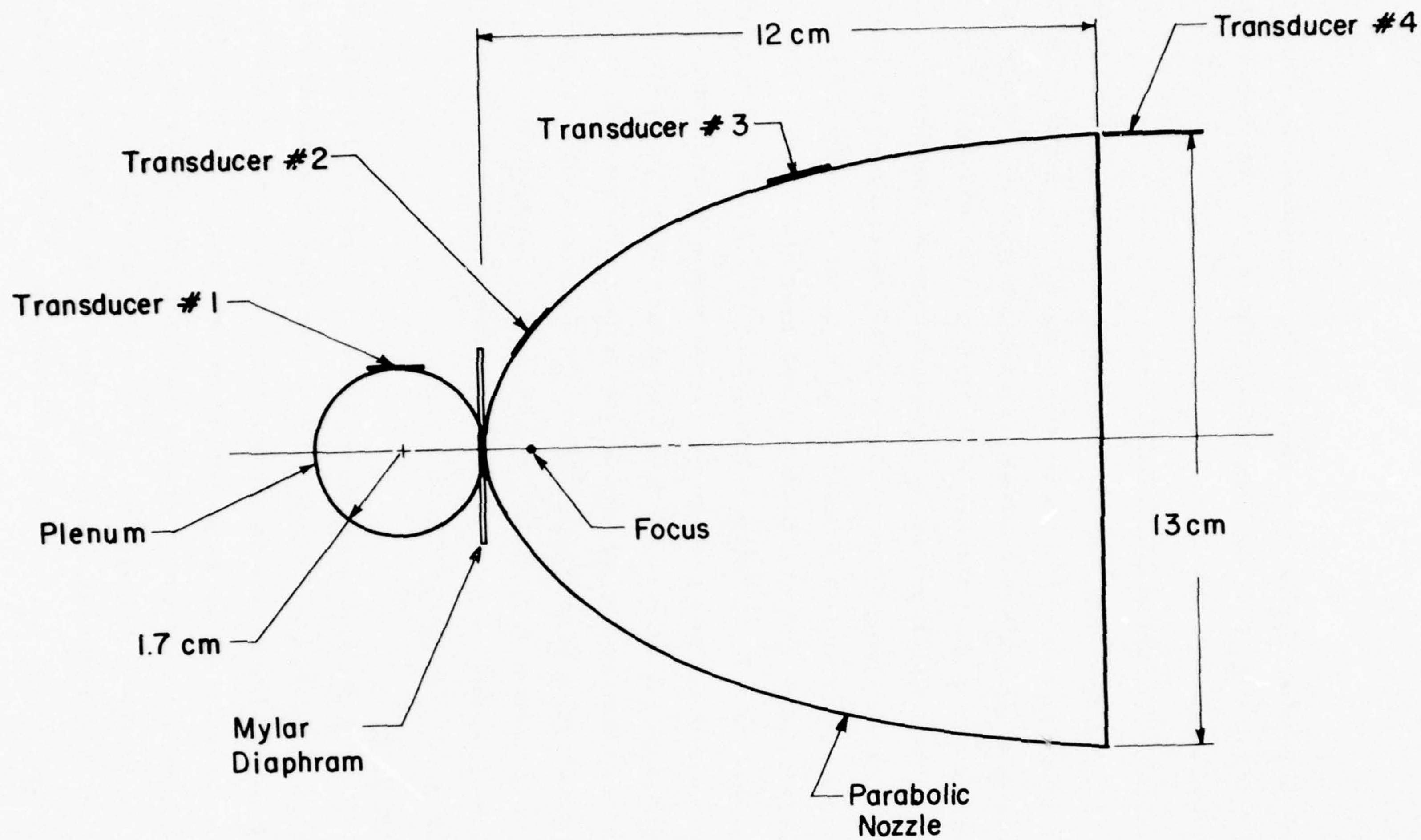

Fig. 22 Parabolic Nozzle Design

experimentally. Again, suggested pressure transducer locations are indicated in Fig. 22 at the plenum wall, the throat, the "breakthrough" radius and the exit plane.

Laser Beam Focusing Requirements

The most important focusing requirement is that a laser-induced breakdown is achieved in the vicinity of the throat. For most of the anticipated propellants a focused laser intensity of $>10^9$ W/cm^2 will yield a breakdown in the 1 atm gas at the throat. The peak power from the above mentioned lasers can be computed from the amount of laser energy in the spike. Using 5 J in a 100 nsec pulse, we obtain a peak power of 50 MW. For the conical nozzle in which the beam is focused externally, mirrors can focus each individual beam to a spot area of 10^{-3} cm^2. Therefore, the peak intensity at the focus will exceed 10^{10} W/cm^2. Achieving a breakdown should not be a problem for conical nozzle experiments. The focusing ability of a parabolic nozzle will depend upon many factors including the surface condition and the precise curvature of the nozzle walls. The external optics becomes simplified, and a series of flats can be used to pass each beam into a nozzle (see Fig. 18). The strength of the laser-induced breakdown is one of the desired measurements to be made using a wall mounted pressure transducer.

Propellant

The choice of a propellant will be dictated by (1) the desire to obtain a high specific impulse, (2) ease of obtaining a breakdown and (3) convenience for laboratory operation. Since it is desirable to use a low molecular weight propellant, most experiments can be performed using helium. A few experiments with hydrogen should be attempted since ultimately hydrogen may be more desirable from a systems viewpoint. The use of other propellants (such as water vapor) that may prove advantageous as a result of systems analyses should be reviewed.

Test Plan

A typical test plan for a possible pulsed laser propulsion experiment is presented in Fig. 23. Before embarking on a series of experiments with multiple laser pulses and propellant flow, however, it is desirable to perform a series of single pulse experiments with only ambient air in the nozzle, similar to the experiments performed in Ref. 4. It was found in Ref. 4 that long laser pulses lead to inefficient conversion of laser power to thrust with a resulting low specific impulse. Since the TEA lasers have short pulses, a series of experiments with no propellant flow should be performed to determine the dependence of the propulsion efficiency on pulse time. These experiments should be performed at various laser energy levels and exit plane pressures. Back[13] has presented a theory for the specific impulse expected from a single blast at the apex of a conical nozzle. Comparisons with this theory for the conical nozzle experiments can be made. In addition, such experiments can be used to calibrate a load cell and examine the focusing ability of the parabolic nozzle configuration.

The test matrix in Fig. 23 has been divided into two parts. The first series of experiments, where specific impulse is the output, is designed to examine the validity of Fig. 8 and Eq. 17. For the experimental conditions enumerated in the previous section each combination of laser energy (E) and time between pulses ($t_p - t_s$) will yield a time averaged delivered power, and using Eq. (17) or Fig. 8, we calculate the expected specific impulse (I_{sp}) presented in the matrix. Experiments should be performed for this variety of laser conditions first in a vacuum, then with increasing exit plane pressure, and with both the conical nozzle and the parabolic nozzle. The second series of experiments, where we want to examine the constant I_{sp} corridor of Fig. 14, is designed to determine the regime of validity of the theoretical model. These experiments should be performed with the laser energy and time between pulses that is specified

Fig. 23 TEST MATRIX

EXPERIMENTS TO BE PERFORMED WITH CONICAL AND PARABOLIC NOZZLES,
EXIT PLANE PRESSURES $p_\infty = 2 \times 10^{-5}$, 10^{-3}, 10^{-1}, 1 ATM.

	E (J) / $t_p - t_s$ (sec)	1	3	5	7	9	11	13	15
SPECIFIC IMPULSE OUTPUT (SEC)	10^{-4}	150	350	350	410	470	510	560	600
	5×10^{-5}	220	380	490	580	660	730	800	850
	10^{-5}	490	850	1100	1300	1480	1640	1780	1900
	E (J) / I_{sp} (sec)	1	3	5	7	9	11	13	15
TIME BETWEEN PULSES FOR CONSTANT I_{sp} (SEC)	800	3.8×10^{-6}	1.1×10^{-5}	1.9×10^{-5}	2.66×10^{-5}	3.4×10^{-5}	4.1×10^{-5}	5×10^{-5}	6×10^{-5} sec
	1000	2.4×10^{-6}	7.3×10^{-6}	1.21×10^{-5}	1.7×10^{-5}	2.2×10^{-5}	2.6×10^{-5}	3.1×10^{-5}	3.6×10^{-5}

to yield a constant specific impulse. Again, the experiments should be performed with both nozzles and at various exit plane pressures to determine the vacuum and atmosphere performance to be expected from the pulsed laser propulsion system.

VIII. SUMMARY AND CONCLUSIONS

A fluid mechanical model to describe the flow within a conical nozzle that is subjected to point energy depositions at the apex of the cone has been developed. The model has been used to assess the concept of pulsed laser propulsion.[4] The specific impulse of a pulsed laser propelled rocket has been obtained as a function of nozzle sonic conditions, the laser energy and the pulse repetition frequency. The results are given by Eq. (17) and illustrated in Fig. 8. Specific impulses of the order of a few thousand seconds may be obtained with moderate energy densities and pulse repetition frequencies. However, these results are valid only for an expansion to a vacuum. The reduction in the thrust due to a finite exit plane pressure may be significant. The finite exit plane pressure may arise due to either the finite ambient pressure, or the finite length of the rocket nozzle. The degradation of the specific impulse due to both of these effects has been assessed.

The relative efficiency (as defined in Eq. 10) of a pulsed propulsion system has been determined and compared to a CW system. This efficiency is based on fluid mechanical considerations only, and the laser absorption mechanisms have not been considered. That is, we have assumed, for both CW and pulsed, that all of the laser energy has been absorbed by the working medium. Results indicate that pulsed laser propulsion is approximately 98% to 99% as efficient as the CW device in converting laser power to thrust. Hence, pulsed laser propulsion appears as versatile and as efficient as the CW technique with the potential advantages of simplicity in engine design and the elimination of possible plasma stability constraints that may be associated with a CW laser propulsion system. Finally, an experiment to test the theoretical model and validate the overall concept has been designed and appears feasible using existing commercially produced lasers.

REFERENCES

1. A. R. Kantrowitz, "Propulsion to Orbit by Ground-Based Lasers", Aeronautics and Astronautics, Vol. 10, No. 5, May 1972, p. 74.

2. A. N. Pirri and R. F. Weiss, "Laser Propulsion", AIAA Paper 72-719, Boston, MA (1972).

3. F. E. Rom and H. A. Putre, "Laser Propulsion", NASA TM-X-2510, April 1972.

4. A. N. Pirri, M. J. Monsler and P. E. Nebolsine, "Propulsion by Absorption of Laser Radiation", AIAA Journal, Vol. 12, No. 9 September 1974, pp. 1254-1261.

5. D. D. Papailiou, ed., "Frontiers in Propulsion Research: Laser, Matter - Antimatter, Exited Helium, Energy Exchange, Thermonuclear Fusion", NASA TM 33-722, Jet Propulsion Laboratory, Pasadena, California, March 1975.

6. L. N. Myrabo, "MHD Propulsion by Absorption of Laser Radiation," Journal of Spacecraft and Rockets, Vol. 13, No. 8, August 1976, pp. 466-472.

7. G. E. Caledonia, P. K. S. Wu and A. N. Pirri, "Radiant Energy Absorption Studies for Laser Propulsion", NASA Report CR-134809, Physical Sciences Inc. Report TR-20, March 1975; also P. K. S. Wu and A. N. Pirri, "Stability of Laser Heated Flows", AIAA Journal, Vol. 14, No. 3, March 1976, pp. 390-392.

8. A. N. Pirri, R. Schlier and D. Northam, "Momentum Transfer and Plasma Formation above a Surface with a High Power CO_2 Laser", Applied Physics Letters, Vol. 21, No. 3, Aug. 1972, pp. 79-81.

9. J. E. Lowder, D. E. Lencioni, T. W. Hilton, and R. J. Hull, "High-Energy Pulsed CO_2 Laser-Target Interaction in Air", Journal of Applied Physics, Vol. 44, No. 6, June 1973, p. 2759.

10. A. N. Pirri, "Theory for Momentum Transfer to a Surface with a High-Power Laser, The Physics of Fluids, Vol. 16, No. 9, Sept. 1973, p. 1435.

11. R. B. Hall, W. E. Maher, and P. S. P. Wei, "An Investigation of Laser-Supported Detonation Waves", AFWL-TR-73-28, June 1973, Air Force Weapons Lab., N. Mexico.

12. L. R. Hettche, J. T. Schriempf, and R. L. Stegman, "Impulse Reaction Resulting from the In-Air Irradiation of Aluminum by a Pulsed CO_2 Laser", Journal of Applied Physics, Vol. 44, No. 9 Sept. 1973, p. 4079.

13. L. H. Back and G. Varsi, "Detonation Propulsion for High Pressure Environments", AIAA Journal, Vol. 12, No. 8, August 1974, p. 1123-1130.

14. L. I. Sedov, Similarity and Dimensional Methods in Mechanics, (M. Holt, ed.), Academic Press, New York, 1959.

15. C. Lahaye, L. Jean and H. Doyle, "Velocity Distributions in the Wake of Spheres", AIAA Journal, Vol. 8, No. 8, August, 1970, pp. 1521.

APPENDIX

SHOCK REFLECTION FROM NOZZLE WALLS

In analyzing the pulsed laser propulsion concept, we have assumed that the nozzles are conical. In reality, the nozzles will have a shape that is other than conical and the blast wave will reflect from the nozzle walls. These shock reflections will create pressure and velocity perturbations in the flow which will degradate the performance of the system. This degradation must be assessed in order to insure that the pulsed system is fluid mechanically as efficient as the CW device.

For simplicity, we will consider the "real nozzle" illustrated in Fig. A-1. The nozzle is assumed to be conical for length R_o, where the curvature is concentrated into a single turn in the wall. The deflection of the wall creates a corner shock, A, to turn the flow parallel to the wall, and a lamda shock, B, which is the reflection of the blast wave from the wall. The shock structure will propagate radially toward the nozzle centerline as the blast wave moves down the nozzle. Ultimately, the shock structure will reflect from the nozzle centerline and form a second normal shock, further complicating the flowfield. Our problem is to first determine that portion of the flowfield which will cause the primary thrust degradation.

Figure A-2 illustrates that portion of the thrust which is generated by the gas between $\eta = 0$, and η. Clearly, 90% of the thrust is generated by the gas between $\eta = 0.6$ and $\eta = 1$. Hence, we are concerned only with shock

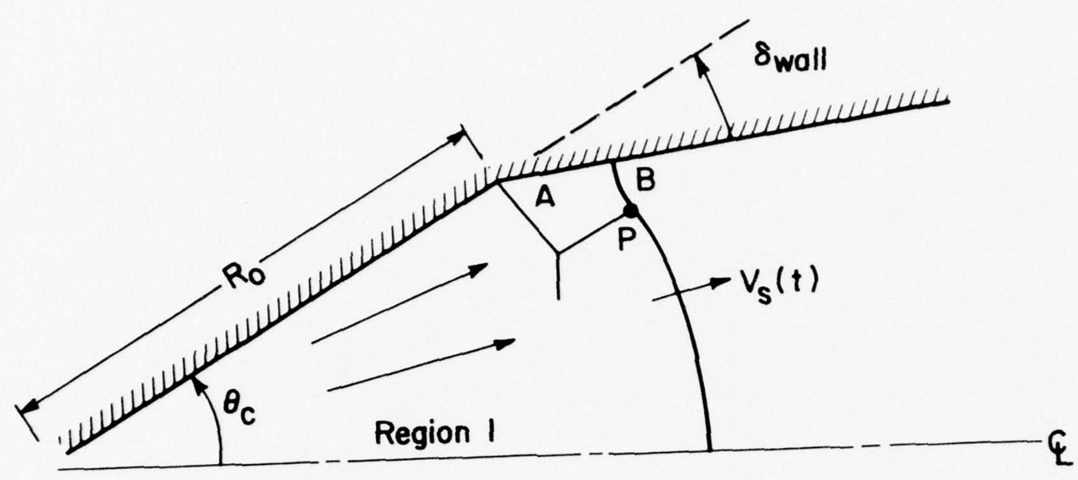

Fig. A-1 Idealized Nozzle Curvature

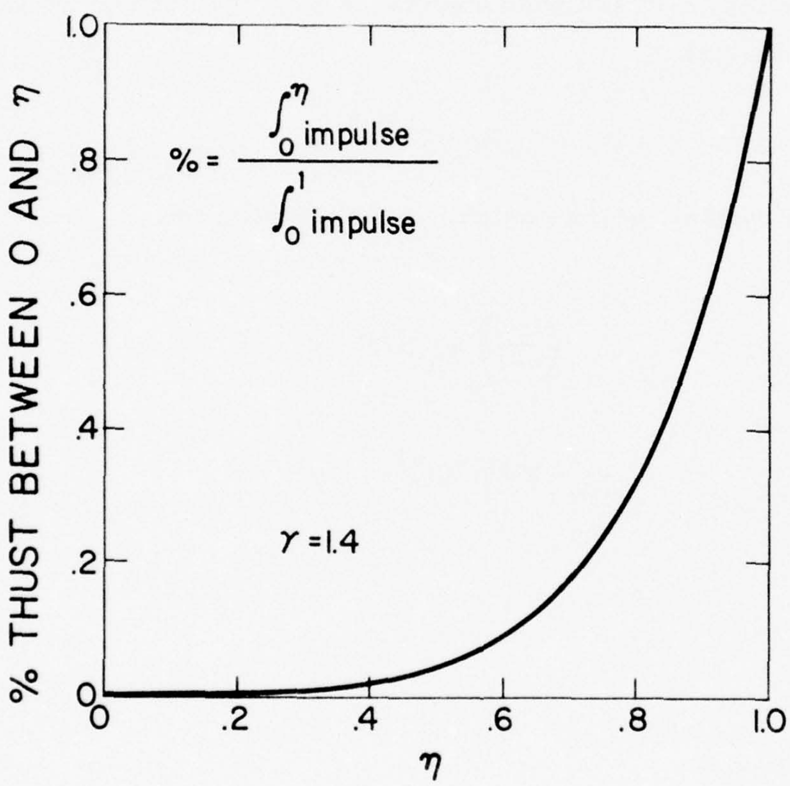

Fig. A-2 Distribution of Thrust in η Space

reflections which occupy that portion of the gas. We will demonstrate that the second normal shock cannot form in the $\eta > 0.6$ region, and the primary fluid mechanical requirement is to model the flowfield illustrated in Fig. A-1.

Region 1 of Fig. A-1 is a zone of silence. The fluid mechanical properties of region 1 have been obtained in Sec. III. The shock radius $R_s(t)$, increases as

$$R_s(t) = At^{2/3} \quad ,$$

where A is a constant of the motion. The fluid velocity is

$$u = \left(\frac{2}{\gamma+1}\right) V_s \, h(\eta) \quad ,$$

where

$$V_s = (2/3)\, A t^{-1/3} \quad ,$$

and

$$h(\eta) \approx \eta \quad ,$$

where

$$\eta = r/R_s(t) \quad .$$

The Mach number of the gas is denoted by

$$M_1 = u/\sqrt{\gamma RT} \doteq \left(\frac{2}{\gamma(\gamma-1)}\right)^{1/2} \eta \quad , \qquad \text{(A-1)}$$

where we have made the approximation that the temperature is constant in the shock profile. Numerical results indicate that Eq. (A-1) is within 5% accuracy for $\gamma = 1.4$ and $0.2 < \eta < 1$.

The relatively low Mach numbers indicated by Eq. (A-1) suggests that the disturbances will be weak and linear theory may be employed. Let us first trace the acoustic waves propagating from wall to determine the nature of the shock interaction zone. These waves are illustrated in Fig. A-3. Wave A is the leading wave and propagates against the mean gas velocity. Wave B is the trailing wave and propagates immediately behind the shock. The two waves represent the limits of the zone of influence of the corner.

To trace the waves through the shock profile, we express the wave velocity in terms of the speed of sound and the mean gas velocity.

$$R_A \frac{d\theta_A}{dt} = -\sqrt{\gamma RT} , \qquad \text{(A-2)}$$

$$\frac{dR_A}{dt} = u - \sqrt{\gamma RT} , \qquad \text{(A-3)}$$

and

$$R_B \frac{d\theta_B}{dt} = -\sqrt{\gamma RT} , \qquad \text{(A-4)}$$

where

$$R_B = R_s(t) .$$

The initial conditions to be imposed on Eqs. (A-2) through (A-4) are: At $t = t_o$, $\theta_A = \theta_B = \theta_C$ and $R_A = R_B = R_o$ where t_o and R_o are related by the arrival of the shock at R_o,

$$R = At_o^{2/3} .$$

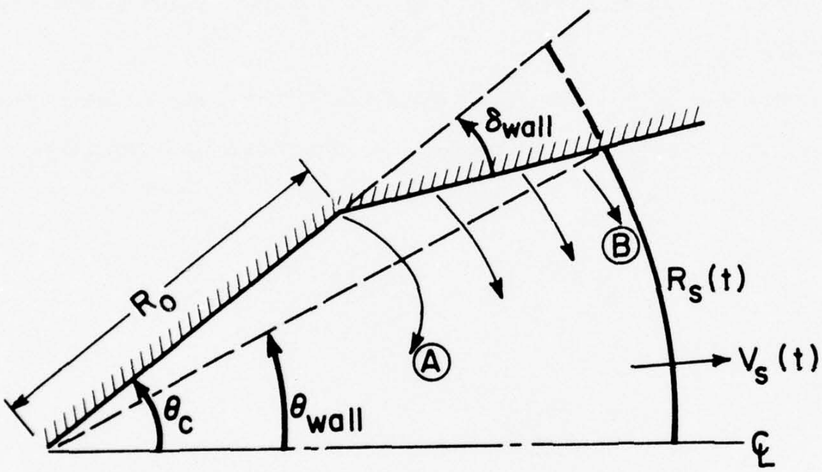

Fig. A-3 Acoustic Waves Propagating From Corner

Denoting t/t_o by τ_1, Eq. (A-3) yields,

$$\frac{R_A}{R_o} = \left(1 + \sqrt{\frac{2\gamma}{\gamma-1}}\right) \tau_1^{\,4/3(\gamma+1)} - \sqrt{\frac{2\gamma}{\gamma-1}}\ \tau_1^{\,2/3} . \qquad \text{(A-5)}$$

Equation (A-5) is illustrated in Fig. A-4. Wave A is initiated in a supersonic flow and travels outward, but with a velocity less than the gas velocity. Eventually the subsonic portion of the shock profile overtakes the wave and allows the wave to propagate to $\eta = 0$. Since most of the thrust is obtained from the gas between $\eta = 0.6$ and $\eta = 1$, we are interested in wave A between $\tau_1 = 1$ and $\tau_1 = 3$ only. The angular propagation of wave A is obtained from Eq. (A-2). For $R_A \approx R_o$, integration yields

$$\theta_A = \theta_C - \frac{\sqrt{2\gamma(\gamma-1)}}{(\gamma+1)} \left(\tau_1^{\,2/3} - 1\right) , \qquad \text{(A-6)}$$

and $\theta_C - \theta_A$ is illustrated in Fig. A-5. Note that in the time of interest ($\tau_1 \leq 3$), wave A propagates less than 30° from the wall. Hence, for cone angles greater than 30°, wave A cannot form a normal shock which would influence that portion of the gas from which the dominant thrust is obtained.

Before we can verify the schematic of the shock structure as illustrated in Fig. A-1, the motion of the trailing wave must be determined. Comparing Eqs. (A-2) and (A-4), we note that $d\theta_A \geq d\theta_B$ because $R_B \geq R_A$. Hence, shock A propagates further from the wall than shock B as indicated in the schematic. However, we must still demonstrate that wave B can escape the wall. That is, we must demonstrate that wave B forms a lamda shock rather than an attached reflection. Integration of Eq. (A-4) yields $\theta_B(\tau_1)$.

$$\theta_B = \theta_C - \frac{2\sqrt{2\gamma(\gamma-1)}}{3(\gamma+1)} \ln \tau_1 \quad . \qquad \text{(A-7)}$$

If we define θ_{wall} as the angle where the initial shock intersects the wall, then the simple geometrical relationship illustrated in Fig. A-3 yields

$$(R_s(t) - R_o)\, \delta_{wall} \doteq (\theta_C - \theta_{wall})\, R_s(t) ,$$

or

$$\theta_{wall} \doteq \theta_C - \left(\frac{\tau_1^{2/3} - 1}{\tau_1^{2/3}} \right) \delta_{wall} \quad . \qquad \text{(A-8)}$$

θ_B and θ_{wall} are compared in Fig. A-6. For $\delta_{wall} \leq 30^\circ$, the wave propagates faster than the wall and must form a detached, or lamda shock as illustrated in Fig. A-1.

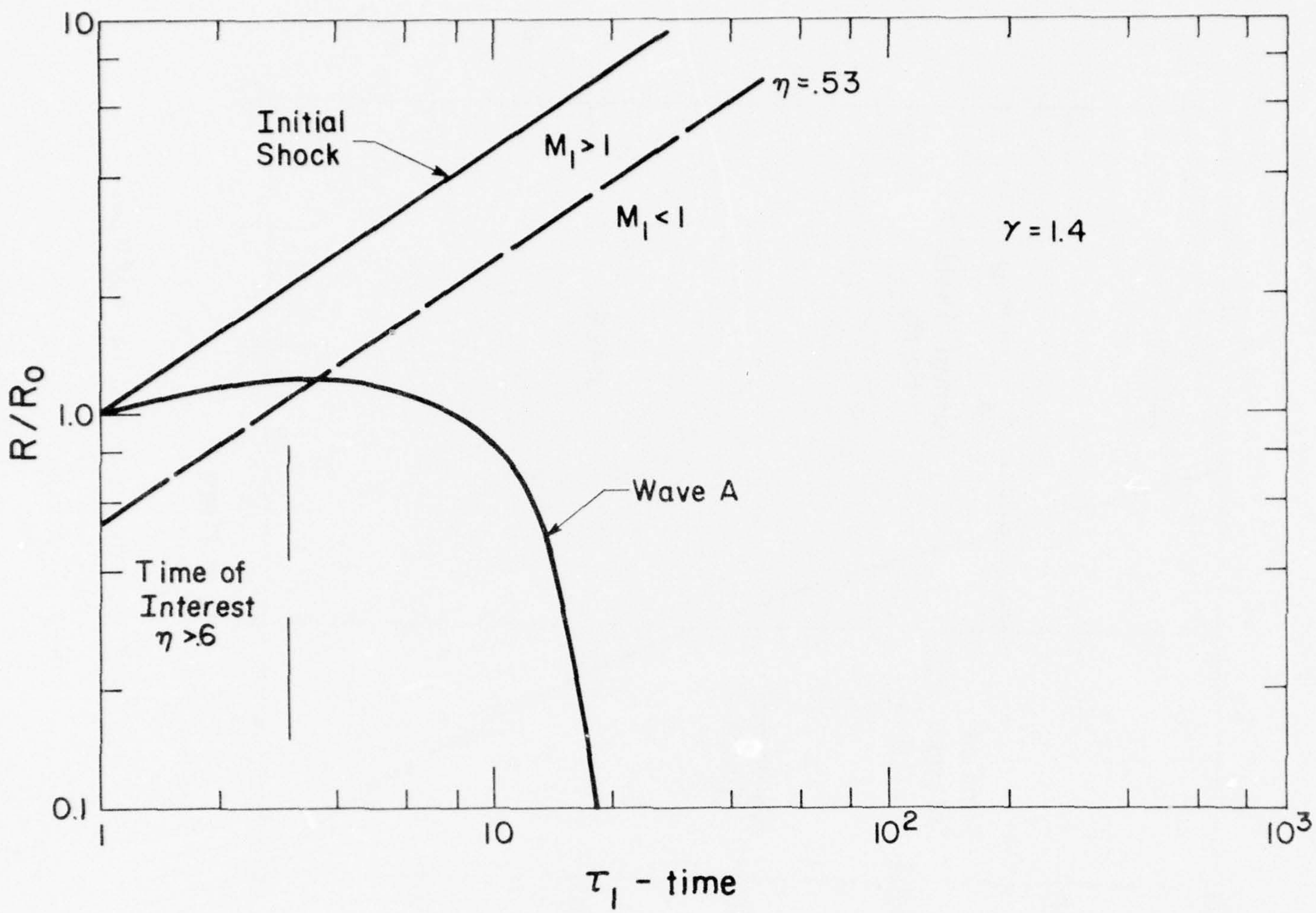

Fig. A-4 Radial Motion of Loading Wave

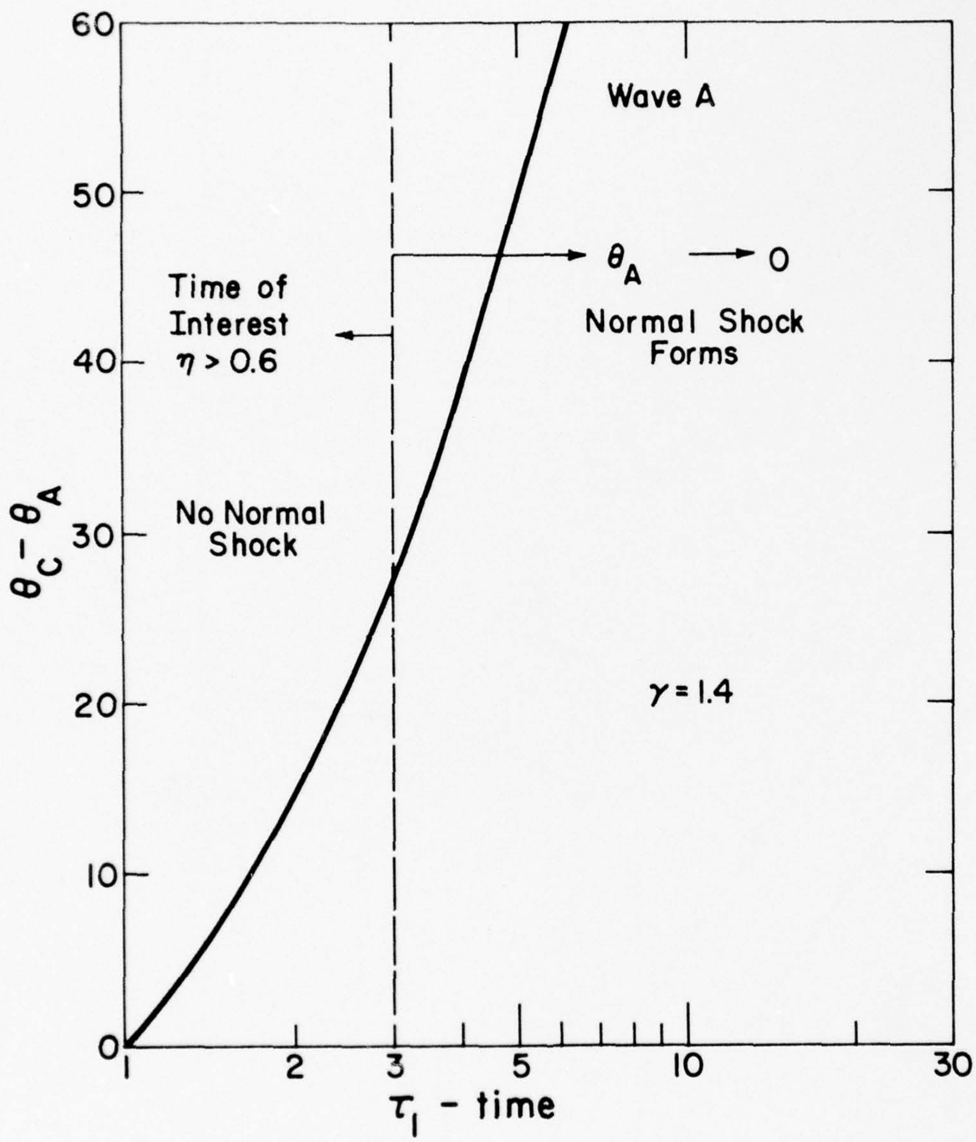

Fig. A-5 Angular Motion of Leading Wave

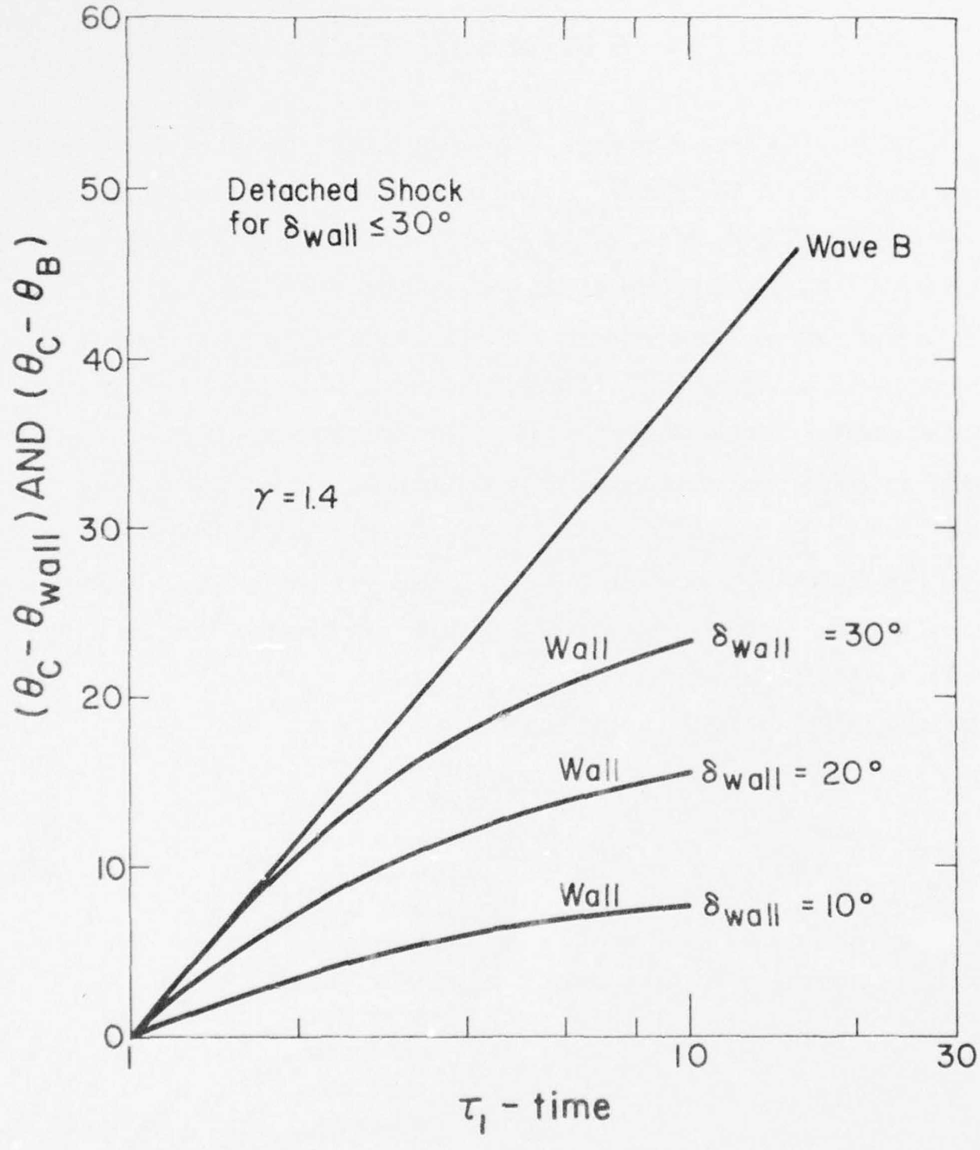

Fig. A-6 Angular Motion of Trailing Wave

LOSS IN THRUST DUE TO SHOCK REFLECTIONS

With the qualification that Fig. A-1 is a meaningful schematic of the shock structure for $\theta_C > 30^o$ and $\delta_{wall} < 30^o$, we will now proceed to analyze the effect of this shock structure on the specific impulse of the pulsed laser propelled rocket. We shall calculate the velocity perturbation, Δu, created by the shocks and demonstrate that the mass average Δu is very small with respect to the mass average of u. Hence, the effect of the shock structure is a small percentage loss in thrust. This will represent an over estimate of the losses because, once the velocity perturbation is created, it does not "freeze" as will be assumed. Rather, the velocity perturbation will decrease as the disturbed region expands to the nozzle exit plane. This effect is neglected in the analysis and the results are clearly an over estimate of the PLP degradation:

The mass average of Δu is defined as

$$\overline{\Delta u} = \int_0^1 \Delta u \left(\frac{dm}{M}\right) , \qquad \text{(A-9)}$$

where M is the total mass released per pulse

$$M = \rho^* u^* \Omega (r^*)^2 (t_p - t_s) , \qquad \text{(A-10)}$$

and Ω is the solid angle of the cone

$$\Omega = 2\pi (1 - \cos \theta_C) .$$

The system degradation due to the reflection of the blast wave from the nozzle wall will now be assessed. We shall assume that the intersection of shock B with the blast wave propagates with the velocity of wave B. Therefore, the location of point P, Fig. A-1, is known for all time and the mass affected by wave B is known for all time. The velocity perturbation created by the shock may be estimated in the Newtonian limit

$$(\Delta u)_B = \left(\frac{2}{\gamma+1}\right) V_s \, \delta_{wall} \, , \qquad \text{(A-11)}$$

where δ_{wall} is the maximum flow deflection angle. The actual flow deflection angle is a function of θ,

$$\delta = \delta_{wall} + \theta_C - \theta .$$

and Eq. (11) is an overestimate of the velocity perturbation. Although this may be a large velocity perturbation, the mass which is affected is a small fraction of the total mass and the mass average Δu will be shown to be small with respect to $\overline{u}_e$.

The mass disturbed by shock B is expressed as

$$dm - \rho_1 V_s 2\pi R_s^2 \sin\theta \, d\theta \, dt,$$

where ρ_1 is the density upstream of the shock. From (A-9) through A-11), we obtain

$$\frac{\overline{\Delta u}}{\bar{u}_e} = m_1 \int_{t_o}^{t_u} \int_{\theta_B(t)}^{\theta_C} (\Delta u)_B V_s \sin\theta \, d\theta \, dt \quad , \tag{A-13}$$

where

$$m_1 = \frac{(\gamma-1)^2}{\sqrt{6}\,\sqrt{t_{max}}\,\sqrt{t_p - t_s}\,(1 - \cos\theta_C)\, I_2 (u^*)^2 (\gamma+1)} \quad ,$$

and t_u, the upper limit of the time integration, corresponds to either the time at which $\delta \to 0$, or the "break through" time, which ever occurs first. It is worth noting that we have inherently assumed that the "break through" radius is greater than R_o, otherwise the shock reflection never forms. For $t_b > t_o$, i.e. for $R_s(t_b) > R_o$, $\overline{\Delta u}$ is non zero.

To evaluate Eq. (A-13), we make the approximations that

$$\sin\theta \approx \sin\theta_C \quad ,$$

and

$$d\theta = \theta_C - \theta_B(t) \quad .$$

Integration of Eq. (A-13) yields

$$\frac{\overline{\Delta u}}{\overline{u}_e} = m_2 \left[3 + \tau_{1u}^{1/3} (\ln \tau_{1u} - 3) \right] , \tag{A-14}$$

where

$$m_2 = \frac{4 \sin \theta_C \sqrt{2\gamma (\gamma - 1)} (\gamma - 1) \delta_{wall}}{3 (\gamma + 1)^2 (1 - \cos \theta_C) I_2 \sqrt{R_s (t_b)/R_o}} ,$$

and τ_{1u} represents either the break through time

$$\tau_{11} = (R_s (t_b)/R_o)^{3/2} ,$$

or the time at which $\delta \rightarrow 0$

$$\tau_{12} = \exp \left(\frac{3 (\gamma + 1) \delta_{wall}}{2\sqrt{2\gamma (\gamma - 1)}} \right) ,$$

which ever occurs first. An upper bound on $\overline{\Delta u}$ may be obtained by assuming that τ_{11} and τ_{12} occur simultaneously. The maximum values of $\overline{\Delta u}/\overline{u}_e$ are illustrated in Fig. A-7. For wall deflection angles above 20°, PLP degradation may be significant. However, this may be reduced by choosing the pulse repetition frequency such that τ_{11} and τ_{12} are not identical. Thus, the shock may "break through" before the degradation is significant. This is illustrated in Fig. A-8 for $\delta_{wall} = 30^{\circ}$. If the break through radius is less than two R_o, less than 10% loss will result. Should we adjust the frequency such that $R_s (t_b) \leq R_o$, shock B never exists and we need consider only the effects of shock A.

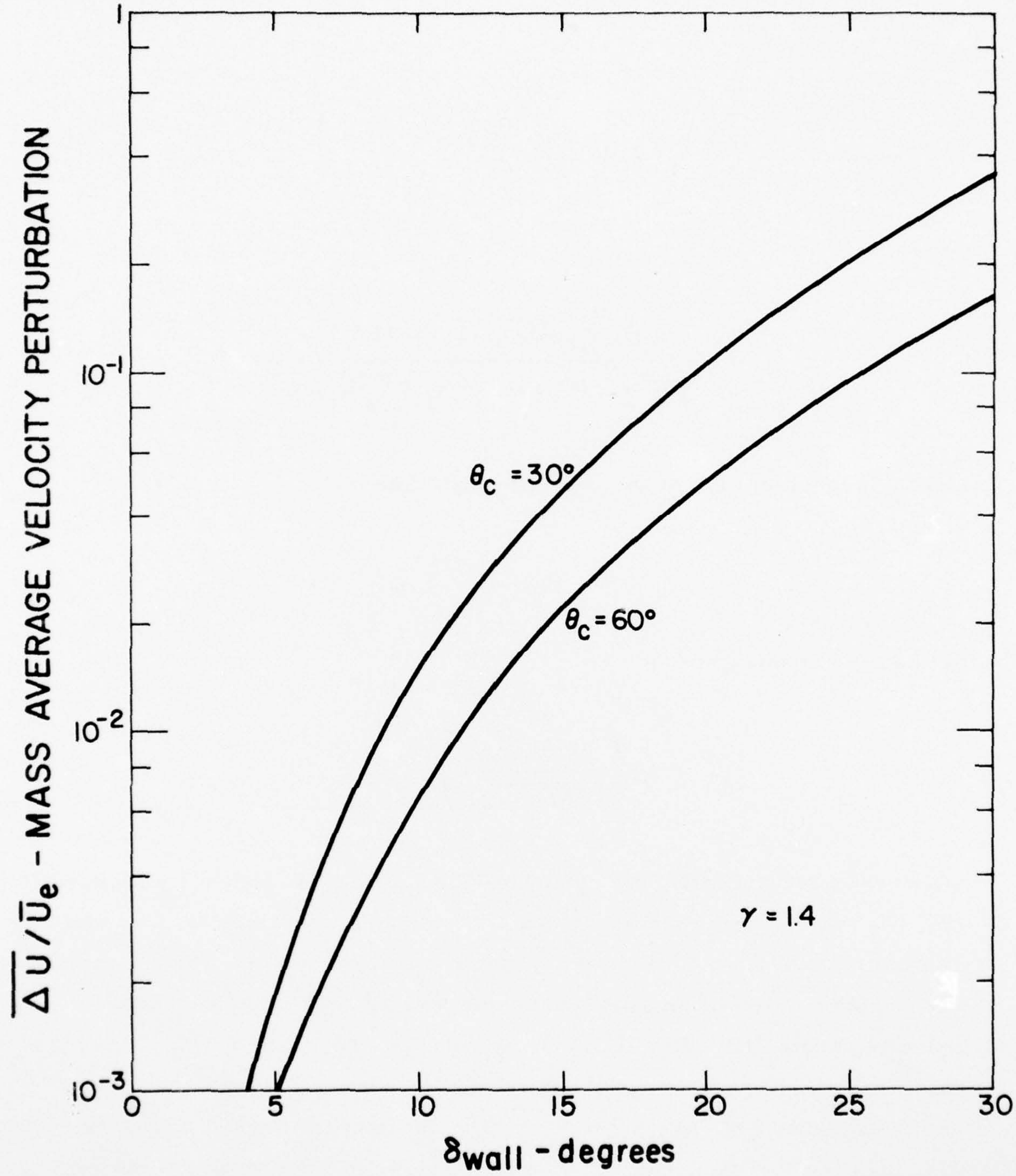

Fig. A-7 Maximum PLP Degradation (Shock B)

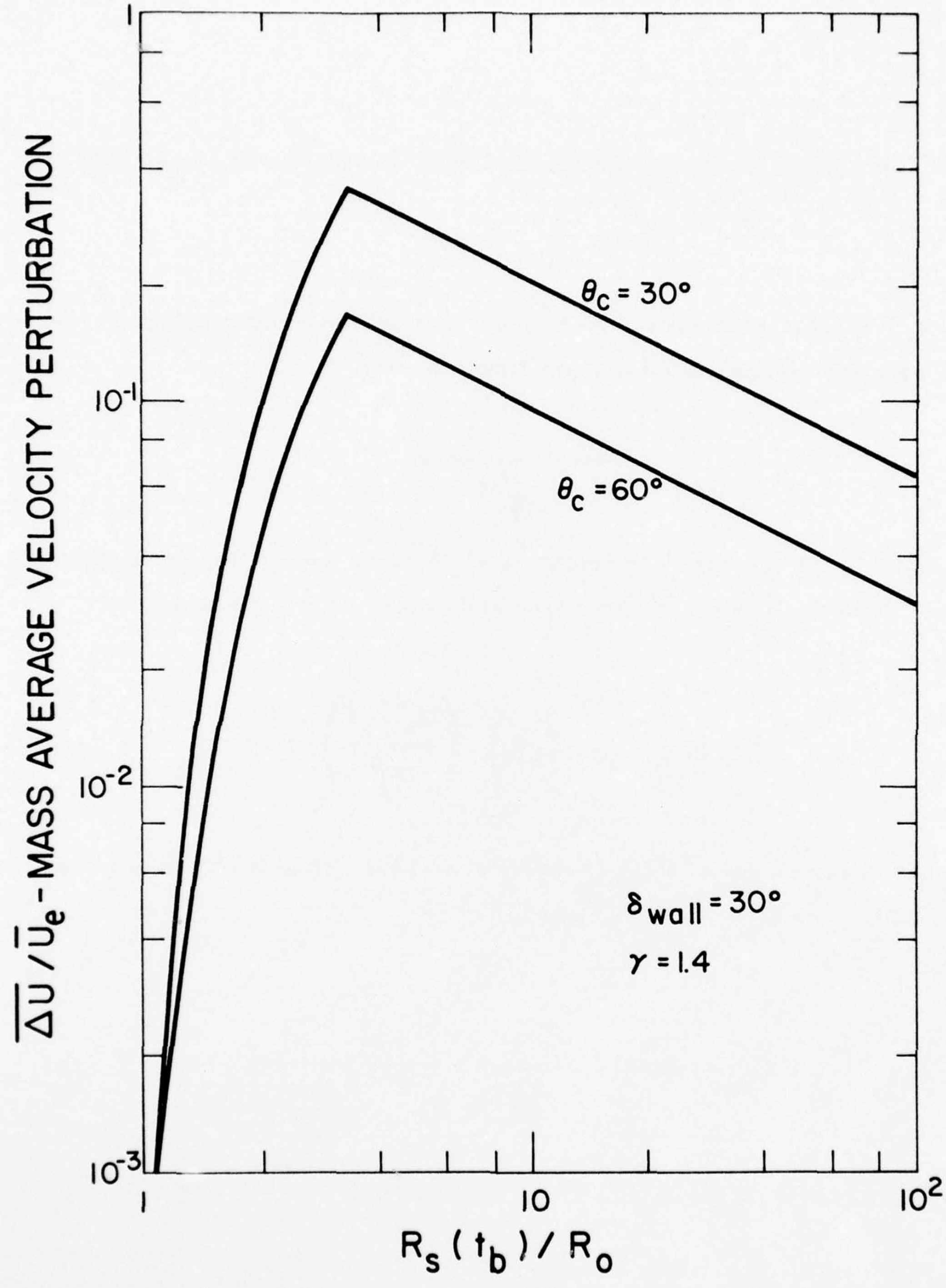

Fig. A-8 Shock B Degradation For $\sigma_{wall} = 30^{\circ}$

The corner shock, A, will deflect each streamline by the amount δ,

$$\delta = \delta_{wall} + \theta - \theta_C \quad ,$$

where θ is evaluated on each streamline. The velocity perturbation associated with each streamline is, from linear theory,

$$\frac{\Delta u}{u} = \frac{\delta}{\sqrt{M_1^2 - 1}} \quad . \tag{A-15}$$

Since Eq. (A-15) becomes unbounded as $M_1 \rightarrow 1$, an upper limit on Δu must be incorporated. The maximum value of Δu occurs for a plane normal shock.

$$(\Delta u)_{max} = \left(\frac{2}{\gamma+1}\right) \left(\frac{M_1^2 - 1}{M_1^2}\right) u \tag{A-16}$$

A realistic composite of Eqs. (A-15) and (A-16) is obtained by taking the reciprocal of the sum of the reciprocals.

$$(\Delta u)_A = k(\theta, \eta)\, u = \frac{\left(M_1^2 - 1\right) \delta u}{\left(M_1^2 - 1\right)^{3/2} + \left(\frac{\gamma+1}{2}\right) M_1^2 \delta} \tag{A-17}$$

The mass average Δu is defined by Eq. (A-9). For shock A, we note that,

$$dm = \rho u \; (2\pi R_o^2 \sin\theta \; d\theta) \; dt \quad ,$$

where we have assumed that shock A remains at $r = R_o$, which is in keeping with the behavior of wave A. The total mass M is that mass which is in the pulse created by the blast wave. Hence, Eq. (A-9) is expressed as

$$\frac{\overline{\Delta u}}{\overline{u}_e} = \frac{4/3\ (\gamma+1)}{\sqrt{R_s(t_b)/R_o}\ (1-\cos\theta_C)\ I_2} \int_{\theta_\ell}^{\theta_C}\int_{\tau_{1\ell}}^{\tau_{1u}} \frac{k(\theta,\eta)\, fh^2 \sin\theta\, d\tau_1\, d\theta}{\tau_1^2} \qquad \text{(A-18)}$$

The choices of $\tau_{1\ell}$ and τ_{1u} are straight forward. We cannot create a velocity perturbation at θ until the wave gets there. Hence, $\tau_{1\ell}$ corresponds to the time at which wave A reaches θ,

$$\tau_{1\ell} = \left[1 + \frac{(\gamma+1)\ (\theta_C - \theta)}{\sqrt{2\gamma\ (\gamma-1)}}\right]^{3/2} .$$

The upper limit, τ_{1u} corresponds to the time at which $M_1 \to 1$. At $r = R_o$, η and τ_1 are related by

$$\eta = \tau_1^{-2/3} . \qquad \text{(A-19)}$$

Hence, from Eqs. (A-1) and (A-19),

$$\tau_{1u} = \left[\frac{2}{\gamma\ (\gamma-1)}\right]^{3/4} .$$

The lower limit on θ is a little more complicated. One choice of θ_{min} corresponds to the value of θ at which $\tau_{1\ell} = \tau_{1u}$. This is denoted by $\theta_{min\,1}$ and corresponds to the minimum value of θ to which wave A can propagate.

$$\theta_{min\,1} = \theta_C - \psi ,$$

where

$$\psi = \frac{2 - \sqrt{2\gamma(\gamma-1)}}{(\gamma+1)} .$$

A second choice for θ_{min} corresponds to the value of θ for which the deflection angle δ, tends to zero.

$$\theta_{min\,2} = \theta_C - \delta_{wall}$$

Clearly, all values of θ must exceed both $\theta_{min\,1}$ and $\theta_{min\,2}$. Hence

$$\theta_{min} = \text{Greater of } (\theta_{min\,1}, \theta_{min\,2}) .$$

The integrand of Eq. (A-18) is a function of η, τ_1 and θ. However, at $r = R_o$, η and τ_1 are related by Eq. (A-19). Therefore, Eq. (A-18) becomes,

$$\frac{\overline{\Delta u}}{\bar{u}_e} = \frac{2/(\gamma+1)}{\sqrt{R_s(t_b)/R_o}\; I_2 (1 - \cos\theta_C)} \int_{\theta_\ell}^{\theta_C} \int_{\eta_{min}}^{\eta_{max}} k(\theta,\eta)\, f(\eta)\, h^2(\eta) \sqrt{\eta}\, \sin\theta \, d\eta \, d\theta ,$$

where

$$\eta_{min} = \left(\frac{\gamma(\gamma-1)}{2}\right)^{1/2} ,$$

and

$$\eta_{max} = \tau_{1\ell}^{-2/3} .$$

The double integration necessary to determine $\overline{\Delta u / \bar{u}_e}$ has been obtained numerically. Results are indicated in Fig. A-9. The mass average velocity perturbation is only 1%. Hence, the loss in thrust due to the corner shock can be no more than 1%. These results are appropriate when the break through radius is identical to R_o. For $R_s(t_b) > R_o$, the effect of shock A decreases but degradation due to shock B increases. The analysis is not appropriate for $R_s(t_b) < R_o$. However the effect of shock A would increase in this situation because the gas Mach number would increase in the expansion from $R_s(t_b)$ to R_o. Although this effect has not been assessed, we can approximate it. For isentropic expansion in a conical nozzle, density decreases as $1/r^2$. Hence, the speed of sound decreases as $r^{1-\gamma}$. Figure A-9 indicates that the mass average velocity can increase by a factor of two. Hence, for an expansion from $R_s(t_b)$ to R_o the Mach number and velocity perturbation can increase by a factor of $2(R_o/R_s(t_b))^{\gamma-1}$. The total degradation due to a 30^o wall is illustrated in Fig. A-10. For $R_s(t_b)/R_o$ between 0.1 and 1.0, less than 10% degradation will result.

In conclusion, we have assessed the problem of PLP degradation by blast wave reflection from the nozzle walls. We have shown that under some circumstances, wall deflection angles of the order of 30^o may cause serious degradation. However, if we properly tune the pulse repetition frequency such that the break through radius is between $R_o/10$ and R_o, it appears that the degradation will be well below 10%. If R_o and $R_s(t_b)$ cannot be maintained in this ratio, degradation may be serious, but a more refined model would be necessary in order to evaluate the effect.

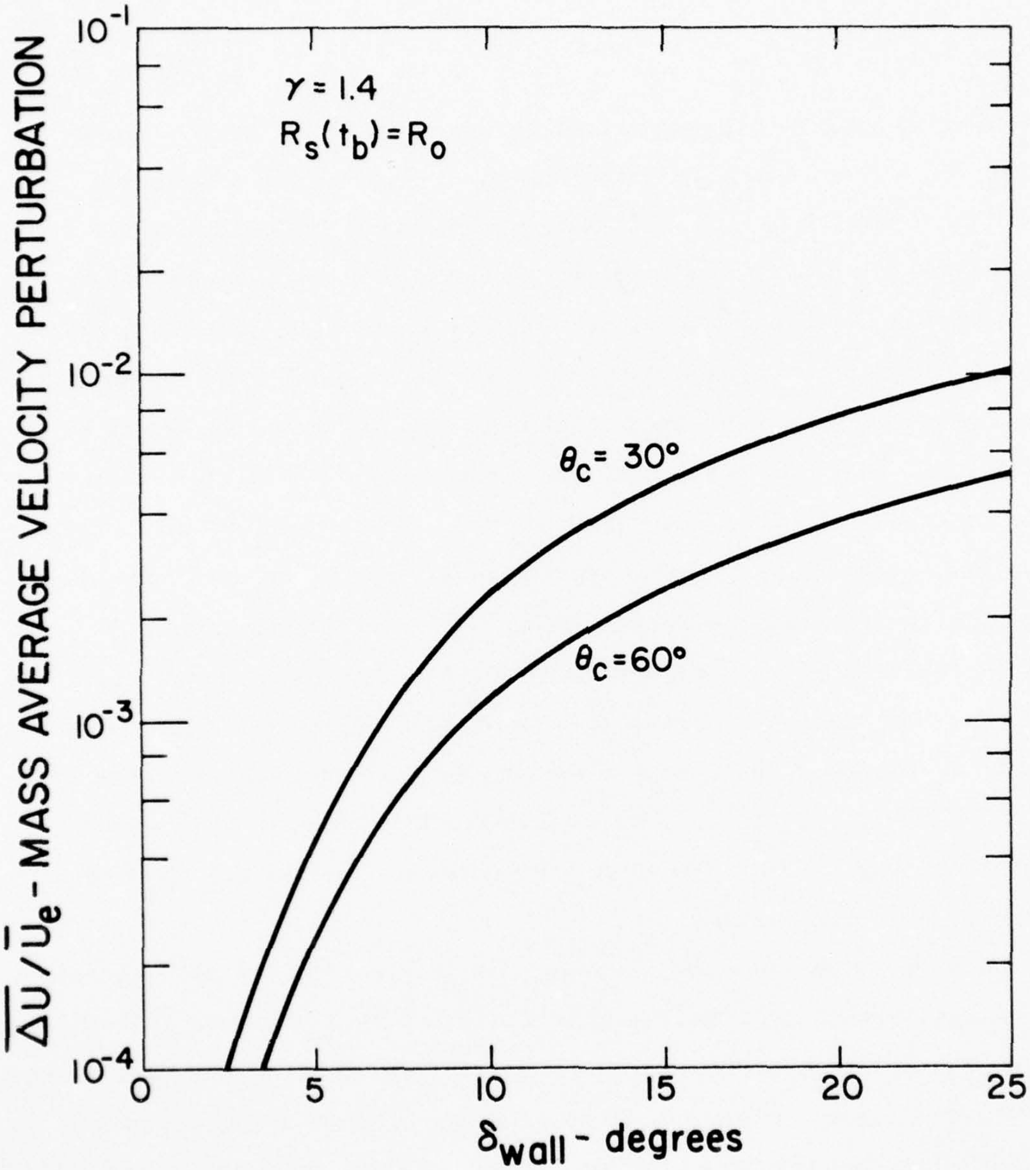

Fig. A-9 PLP Degradation - Shock A

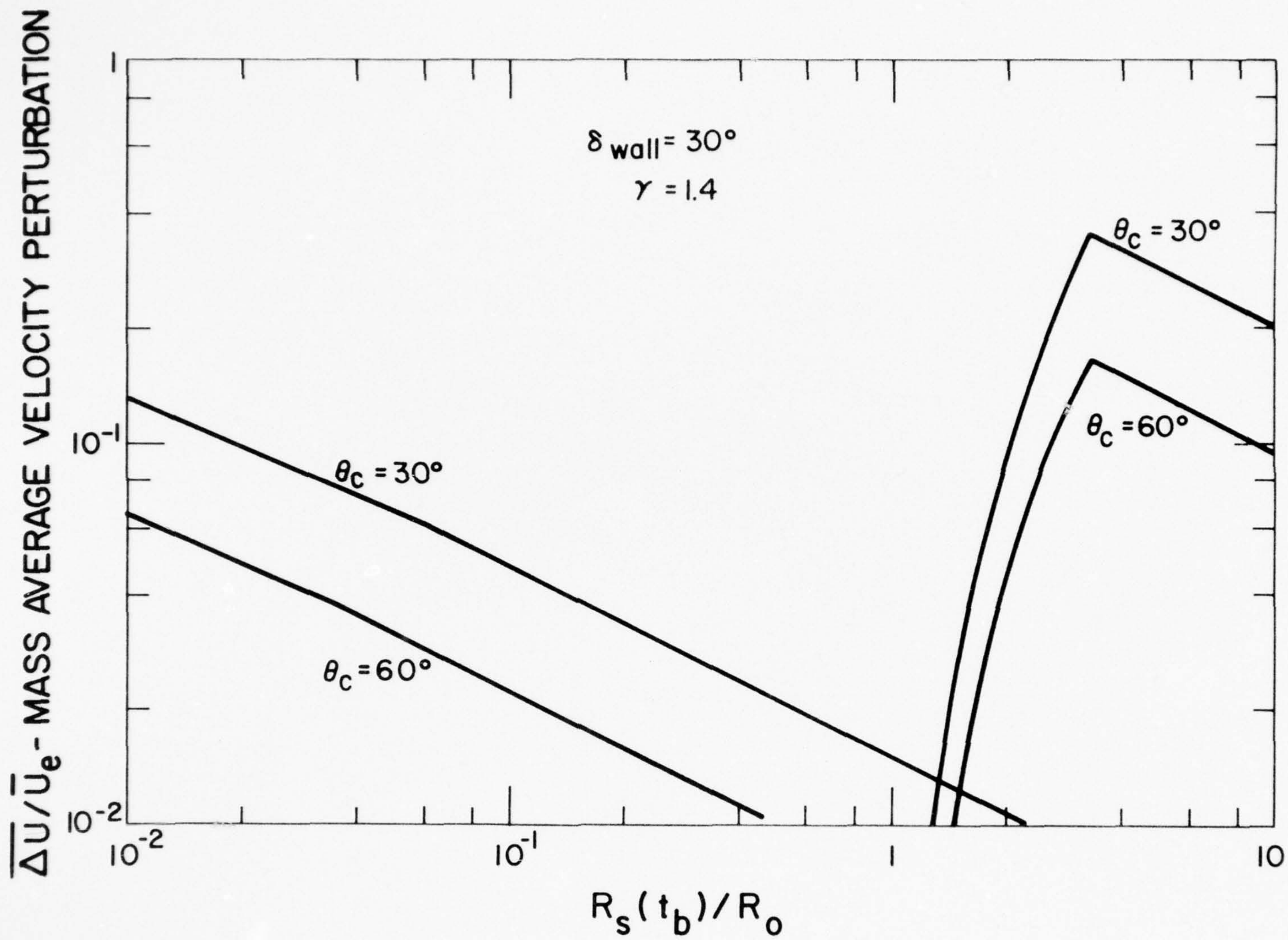

Fig. A-10 Total Degradation for 30° Wall

DISTRIBUTION LIST
FOR
FINAL REPORT

Contract No. N00014-76-C-0738

Scientific Officer Office of Naval Research 495 Summer St. Boston, MA 02210 ATTN: Dr. Al Wood (DOD Code N00014)	1 copy
Scientific Officer c/o Physical Sciences Division Office of Naval Research 800 N. Quincy Street Arlington, VA 22217 ATTN: Dr. W. J. Condell (Code 421)	1 copy
Defense Contract Administration Services District, Boston 666 Summer Street Boston, MA 02210 ATTN: Mr. Robert D. Wholey Administrative Contracting Officer	1 copy
Director, Naval Research Laboratory Washington, D.C. 20375 ATTN: Code 2627	6 copies
Office of Naval Research Branch Office Department of the Navy 495 Summer St. Boston, MA 02210 ATTN: DOD Code N62879	1 copy
Defense Advanced Research Projects Agency 1200 Wilson Boulevard Arlington, VA 22209 ATTN: DOD Code HX1241	1 copy

AD-A033 887   ALUMINIUM FRANCAIS PARIS*   F/G 20/5
THE FLUID MECHANICS OF PULSED LASER PROPULSION.(U)
JUL 76 A N PIRRI, G A SIMONS, P E NEBOLSINE   N00014-76-C-0738

UNCLASSIFIED   PSI-TR-60   NL

2 OF 2
ADA033887

END

DATE
FILMED
2 -77

Office of Naval Research Department of the Navy Attn: Physics Program Arlington, Virginia 22217	3 copies
Naval Research Laboratory Department of the Navy Attn: Technical Library Washington, D. C. 20375	1 copy
Office of the Director of Defense Research and Engineering Information Office Library Branch The Pentagon Washington, D. C. 20301	1 copy
U. S. Army Research Office Box CM, Duke Station Durham, N. C. 27706	1 copy
Defense Documentation Center Cameron Station Alexandria, VA 22314	12 copies
Defender Information Analysis Center Battelle Memorial Institute 505 King Avenue Columbus, OH 43201	1 copy
Commanding Officer Office of Naval Research Branch Office 536 South Clark Street Chicago, IL 60615	1 copy
New York Area Office Office of Naval Research Attn: Dr. Irving Rowe 715 Broadway (5th Floor) New York, N. Y. 10003	1 copy
San Francisco Area Office Office of Naval Research 760 Market Street, Room 447 San Francisco, CA 94102	1 copy
Air Force Office of Scientific Research Department of the Air Force Washington, D. C. 22209	1 copy

Office of Naval Research Branch Office | 1 copy
Attn: Dr. Robert Behringer
1030 East Green Street
Pasadena, CA 91106

Code 102 1P (ONRL) | 6 copies
Office of Naval Research
800 N. Quincy Street
Arlington, VA 22217

Defense Advanced Research Projects Agency | 1 copy
Attn: Strategic Technology Office
1400 Wilson Blvd.
Arlington, VA 22209

Office Director of Defense | 1 copy
Research & Engineering
Attn: Ass't. Dir (Space and Advanced Systems)
The Pentagon
Washington, D. C. 20301

Office of the Ass't Secretary of Defense | 1 copy
Attn: Mr. Gerald R. McNichols
System Analysis (Strategic Programs)
Washington, D. C. 20301

U. S. Arms Control and Disarmament Agency | 1 copy
Attn: Dr. Charles Henkin
Dept. of State Bldg., Rm. 4931
Washington, D. C. 20451

Energy Research Development Agency | 1 copy
Division of Military Applications
Washington, D. C. 20545

National Aeronautics and Space Administration | 1 copy
Lewis Research Center
Attn: Dr. John W. Dunning, Jr.
(Aerospace Res. Engineer)
Cleveland, OH 44135

National Aeronautics & Space Administration | 1 copy
Code RR, FOB 10B
600 Independence Ave., SW
Washington, D. C. 20546

National Aeronautics and Space Administration | 1 copy
Ames Research Center
Attn: Dr. Kenneth W. Billman
Moffett Field, CA 94035

Department of the Army
Office of the Chief of RD&A
Washington, D. C. 20310
Attn: DARD-DD — 1 copy
DAMA-WSM-T — 1 copy

Department of the Army — 1 copy
Office of the Deputy Chief of Staff
for Operations & Plans
Attn: DAMO-RQD
Washington, D. C. 20310

Ballistic Missile Defense Program Office (BMDPO) — 1 copy
The Commonwealth Building
Attn: Mr. Albert J. Bast, Jr.
1300 Wilson Blvd.
Arlington, VA 22209

U. S. Army Missile Command — 2 copies
Research and Development Division
Attn: Army High Energy Laser Programs
Redstone Arsenal, ALA 35809

Commander — 1 copy
Rock Island Arsenal
Attn: SARRI-LR, Mr. J. W. McGarvey
Rock Island, IL 61201

Commanding Officer — 1 copy
U. S. Army Mobility Equipment R&D Center
Attn: SMEFB-MW
Ft. Belvoir, VA 22060

Commander — 1 copy
U. S. Army Armament Command
Attn: AMSAR-RDT
Rock Island, IL 61201

Director
Ballistic Missile Defense Advanced Technology Center
P. O. Box 1500
Huntsville, AL 35807
Attn: ATC-O — 1 copy
ACT-T — 1 copy

Commander — 1 copy
U. S. Army Material Command
Attn: Mr. Paul Chernoff (AMCRD-T)
Alexandria, VA 22304

Commanding General U. S. Army Munitions Command Attn: Mr. Gilbert F. Chesnov (AMSMU-R) Dover, NH 17801	1 copy
Director U. S. Army Ballistics Res. Lab Attn: Dr. Robert Eichenberger Aberdeen Proving Ground, MD 21005	1 copy
Commandant U. S. Army Air Defense School Ft. Bliss, TX 79916	
Attn: Air Defense Agency	1 copy
ATSA-CTD-MS	1 copy
Commanding General U. S. Army Combat Dev. Command Attn: Director of Material, Missile Div. Ft. Belvoir, VA 22060	1 copy
Commander U. S. Army Training & Doctrine Command Attn: ATCD-CF Ft. Monroe, VA 23651	1 copy
Commander U. S. Army Frankford Arsenal Attn: Mr. M. Elnick SARFA-FCD Bldg. 201-3 Philadelphia, PA 19137	1 copy
Commander U. S. Army Electronics Command Attn: AMSEL-CT-L, Dr. R. G. Buser Ft. Monmouth, NJ 07703	1 copy
Commander U. S. Army Combined Arms Combat Developments Activity Ft. Leavenworth, KS 66027	1 copy
National Security Agency Attn: R. C. Foss A763 Ft. Geo. G. Meade, MD 20755	1 copy
Deputy Commandant for Combat & Training Developments U. S. Army Ordnance Center and School Attn: ATSL-CTD-MS-R Aberdeen Proving Ground, MD 21005	1 copy

Commanding Officer USACDC CBR Agency Attn: CDCCBR-MR (Mr. F. D. Poer) Ft. McClellan, AL 36201	1 copy
Department of the Navy Office of the Chief of Naval Operations Attn: (OP 982F3) The Pentagon 5C739 Washington, D. C. 20350	1 copy
Office of Naval Research Branch Office Attn: Dr. Fred Quelle 495 Summer Street Boston, MA 02210	1 copy
Department of the Navy Deputy Chief of Navy Material (Dev.) Attn: Mr. R. Gaylord (MAT 032B) Washington, DC 20360	1 copy
Naval Missile Center Attn: Gary Gibbs (Code 5352) Point Mugu, CA 93042	1 copy
Naval Research Laboratory Washington, D. C. 20375	
Attn: (Code 5503-EOTPO)	1 copy
Dr. P. Livingston - Code 5560	1 copy
Dr. A. I. Schindler - Code 6000	1 copy
Dr. H. Shenker - Code 5504	1 copy
Mr. D. J. McLaughlin - Code 5560	1 copy
Dr. John L. Walsh - Code 5503	1 copy
High Energy Laser Project Office Department of the Navy Naval Sea Systems Command Attn: CAPT A. Skolnick, USN (PM 22) Washington, DC 20360	1 copy
Superintendent Naval Postgraduate School Attn: Library (Code 2124) Monterey, CA 93940	1 copy
Navy Radiation Technology Air Force Weapons Lab (NLO) Kirtland AFB, NM 87117	1 copy

Naval Surface Weapons Center
White Oak
Silver Spring, MD 20910
Attn: Dr. Leon H. Schindel (Code 310) 1 copy
Dr. E. Leroy Harris (Code 313) 1 copy
Mr. K. Enkenhaus (Code 034) 1 copy
Mr. J. Wise (Code 047) 1 copy
Technical Library 1 copy

U. S. Naval Weapons Center 1 copy
Attn: Technical Library
China Lake, CA 93555

HQ USAF (AF/RDPS) 1 copy
Attn: LT COL A. J. Chiota
The Pentagon
Washington, DC 20330

HQ AFSC/XRLW 1 copy
Attn: MAJ J. M. Walton
Andrews AFB
Washington, DC 20331

HQ AFSC (DLCAW) 1 copy
Attn: MAJ H. Axelrod
Andrews AFB
Washington, DC 20331

Air Force Weapons Laboratory
Kirtland AFB, NM 87117
Attn: LR 1 copy
AL 1 copy

HQ SAMSO (XRTD) 1 copy
Attn: LT Dorian DeMaio (XRTD)
P. O. Box 92960, Worldway Postal Center
Los Angeles, CA 90009

AF Avionics Lab (TEO) 1 copy
Attn: Mr. K. Hutchinson
Wright Patterson AFB, OH 45433

Dept of the Air Force 1 copy
Air Force Materials Lab. (AFSC)
Attn: MAJ Paul Elder (LPS)
Laser Window Group
Wright Patterson AFB, OH 45433

HQ Aeronautical Systems Div. Attn: XRF - Mr. Clifford Fawcett Wright Patterson AFB, OH 45433	1 copy
Rome Air Development Command Griffiss AFB Attn: Mr. R. Urtz (OCSE) Rome, NY 13440	1 copy
HQ Electronics Systems Div. (ESL) L. G. Hanscom Field Bedford, MA 01730 Attn: Mr. Alfred E. Anderson (XRT)	 1 copy
Technical Library	1 copy
Air Force Rocket Propulsion Lab. Attn: B. R. Bornhorst, (LKCG) Edwards AFB, CA 93523	1 copy
Air Force Aero Propulsion Lab. Attn: COL Walter Moe (CC) Wright Patterson AFB, OH 45433	1 copy
Dept. 6f the Air Force Foreign Technology Division Attn: PDTN Wright Patterson AFB, OH 45433	1 copy
Commandant of the Marine Corps Scientific Advisor (Code RD-1) Washington, DC 20380	1 copy
Aerospace Research Labs., (AP) Attn: LT COL Max Duggins Wright Patterson AFB, OH 45433	1 copy
Defense Intelligence Agency Attn: Mr. Seymour Berler (DTIB) Washington, DC 20301	1 copy
Central Intelligence Agency Attn: Mr. Julian C. Nall Washington, D. C. 20505	1 copy
Analytic Services, Inc. Attn: Dr. John Davis 5613 Leesburg Pike Falls Church, VA 22041	1 copy

Aerospace Corp. Attn: Dr. G. P. Millburn P. O. Box 92957 Los Angeles, CA 90009	1 copy
Airesearch Manuf. Co. Attn: Mr. A. Colin Stancliffe 9851-9951 Sepulveda Blvd. Los Angeles, CA 90009	1 copy
Atlantic Research Corp. Attn: Mr. Robert Naismith Shirley Highway at Edsall Road Alexandria, VA 22314	1 copy
AVCO Everett Research Lab. 2385 Revere Beach Parkway Everett, MA 02149	
Attn: Dr. George Sutton	1 copy
Dr. Jack Daugherty	1 copy
Battelle Columbus Laboratories Attn: Mr. Fred Tietzel (STPIAC) 505 King Avenue Columbus, OH 43201	1 copy
Bell Aerospace Co. Attn: Dr. Wayne C. Solomon Buffalo, NY 14240	1 copy
Boeing Company Attn: Mr. M. I. Gamble (2-,460, MS 8C-88) P. O. Box 3999 Seattle, WA 98124	1 copy
Electro-Optical Systems Attn: Dr. Andrew Jensen 300 N. Halstead Pasadena, CA 91107	1 copy
ESL, Inc. Attn: Arthur Einhorn 495 Java Drive Sunnyvale, CA 94086	1 copy
General Electric Co. Space Division Attn: Dr. R. R. Sigismonti P. O. Box 8555 Philadelphia, PA 19101	1 copy

General Electric Co. Attn: Mr. D. G. Harrington (Rm. 1044) 100 Plastics Avenue Pittsfield, MA 01201	1 copy
General Research Corp. Attn: Dr. R. Holbrook P. O. Box 3587 Santa Barbara, CA 93105	1 copy
General Research Corp. Attn: Dr. Giles F. Crimi 1501 Wilson Blvd., Suite 700 Arlington, VA 22209	1 copy
Hercules, Inc. Industrial System Dept. Attn: Dr. R. S. Voris Wilmington, DE 19899	1 copy
Hercules, Inc. Attn: Dr. Ralph R. Preckel P. O. Box 210 Cumberland, MD 21502	1 copy
Hughes Research Labs Attn: Dr. D. Forster 3011 Malibu Canyon Road Mailbu, CA 90265	1 copy
Hughes Aircraft Co. Aerospace Group - Systems Division Attn: Dr. Jack A. Alcalay Canoga Park, CA 91304	1 copy
Hughes Aircraft Co. Attn: Dr. William Yates Centinela and Teale Streets Bldg. 6, MS E-125 Culver City, CA 90230	1 copy
Institute for Defense Analyses Attn: Dr. Alvin Schnitzler 400 Army-Navy Drive Arlington, VA 22202	1 copy
Johns Hopkins University Applied Physics Lab Attn: Dr. Albert M. Stone 8621 Georgia Avenue Silver Spring, MD 20910	1 copy

Lawrence Livermore Laboratory P. O. Box 808 Livermore, CA 94550 Attn: Dr. R. E. Kidder	1 copy
Dr. E. Teller	1 copy
Dr. Joe Fleck	1 copy
Los Alamos Scientific Laboratory Attn: Dr. Keith Boyer P. O. Box 1663 Los Alamos, NM 87544	1 copy
Lulejian and Associates, Inc. Del Amo Financial Center 21515 Hawthorne Blvd. - Suite 500 Torrance, CA 90503	1 copy
Lockheed Palo Alto Res. Lab. Attn: L. R. Lunsford Orgn. 52-24, Bldg. 201 3251 Hanover St. Palo Alto, CA 94303	1 copy
Mathematical Sciences Northwest, Inc. Attn: Dr. Abraham Hertzberg P. O. Box 1887 Bellevue, WN 98009	1 copy
Martin Marietta Corp. Attn: Mr. Stewart Chapin P. O. Box 179 Mail Station 0471 Denver, CO 80201	1 copy
Massachusetts Institute of Technology Lincoln Laboratory P. O. Box 73 Lexington, MA 02173 Attn: Dr. S. Edelberg	1 copy
Dr. L. C. Marquet	1 copy
Mc Donnell Douglas Astronautics Co. Attn: Mr. P. L. Klevatt Dept. A3-830-BBFO, M/S 9 5301 Bolsa Avenue Huntington Beach, CA 92647	1 copy

Mc Donnell Douglas Research Labs — 1 copy
Attn: Dr. D. P. Ames
Dept. 220, Box 516
St. Louis, MO 63166

MITRE Corp. — 1 copy
Attn: Mr. A. C. Cron
P. O. Box 208
Bedford, MA 01730

North American Rockwell Corp. — 1 copy
Autonetics Div.
Attn: Mr. T. T. Kumagi
C/476 Mail Code HA18
Anaheim, CA 92803

Northrop Corp. — 1 copy
Attn: Dr. Gerard Hasserjian
Laser Systems Dept.
3401 West Broadway
Hawthorne, CA 90250

Dr. Anthony N. Pirri — 1 copy
Physical Sciences, Inc.
18 Lakeside Office Park
Wakefield, MA 01880

RAND Corp. — 1 copy
Attn: Dr. C. R. Culp/Mr. G. A. Carter
1700 Main Street
Santa Monica, CA 90406

Raytheon Co. — 1 copy
Attn: Dr. F. A. Horrigan (Res. Div.)
28 Seyon Street
Waltham, MA 02154

Raytheon Co. — 1 copy
Attn: Dr. C. Sonnenschien (Equip. Div.)
Boston Post Road
Sudbury, MA 01776

Raytheon Co. — 1 copy
Bedford Labs, Missile Systems Div.
Attn: Dr. H. A. Mehlhorn
Bedford, MA 01730

Riverside Research Institute
80 West End Street
New York, NY 10023
Attn: Dr. L. H. O'Neill — 1 copy
Dr. John Bose — 1 copy
(HPEGL Library) — 1 copy

R&D Associates, Inc. — 1 copy
Attn: Dr. R. E. LeLevier
P. O. Box 3580
Santa Monica, CA 90431

Rockwell International Corporation — 1 copy
Rocketdyne Division
Albuquerque District Office
Attn: C. K. Kraus, Mgr.
3636 Menaul Blvd., NE, Suite 211
Albuquerque, NM 87110

SANDIA Corp. — 1 copy
Attn: Dr. Al Narath
P. O. Box 5800
Albuquerque, NM 87115

Stanford Research Institute
Attn: Dr. F. T. Smith — 1 copy
Menlo Park, CA 94025

Science Applications, Inc. — 1 copy
Attn: L. Peckam
1911 N. Ft. Meyer Drive
Arlington, Va. 22209

Science Applications, Inc. — 1 copy
Attn: R. E. Meredith
P. O. Box 328
Ann Arbor, MI 48103

Science Applications, Inc. — 1 copy
Attn: R. Greenberg
6 Preston Court
Bedford, MA 01703

Science Applications, Inc. — 1 copy
Attn: Dr. John Asmus
P. O. Box 2351
La Jolla, CA 92037

Systems, Science and Software Attn: Alan F. Klein P. O. Box 1620 La Jolla, CA 92037	1 copy
Systems, Consultants Inc. Attn: Dr. R. B. Keller 1050 31st Street, NW Washington, DC 20007	1 copy
Thiokol Chemical Corp. WASATCH Division Attn: Mr. J. E. Hansen P. O. Box 524 Brigham City, UT 84302	1 copy
TRW Systems Group Attn: Nr. Norman Campbell One Space Park Bldg. R-1, Rm. 1050 Redondo Beach, CA 90278	1 copy
United Technologies Research Center Attn: Mr. G. H. McLafferty 400 Main Street East Hartford, CT 06108	3 copies
United Technologies Research Center Pratt and Whitney Acft. Div. Florida R&D Center West Palm Beach, FL 33402	
Attn: Dr. R. A. Schmidtke	1 copy
Mr. Ed Pinsley	1 copy
VARIAN Associates EIMAC Division Attn: Mr. Jack Quinn 301 Industrial Way San Carlos, CA 94070	1 copy
Vought Systems Division LTV Aerospace Corp. Attn: Mr. F. G. Simpson, MS 254142 P. O. Box 5907 Dallas, TX 75222	1 copy
Westinghouse Electric Corp. Defense and Space Center Attn: Mr. W. F. List Balt-Wash. International Airport - Box 746 Baltimore, MD 21203	1 copy

Westinghouse Research Labs Attn: Dr. E. P. Riedel Beulah Road, Churchill Boro Pittsburgh, PA 15235	1 copy
United Technologies Research Center Attn: A. J. DeMaria East Hartford, CT 06108	1 copy
Airborne Instruments Laboratory Attn: F. Pace Walt Whitorian Road Melville, NY 11746	1 copy
General Electric R&D Center Attn: Dr. Donald White Schenectady, NY 12305	1 copy
Cleveland State University Attn: Dean Jack Soules Cleveland, OH 44115	1 copy
EXXON Research and Engineering Co. Attn: D. Grafstein P. O. Box 8 Linden, NJ 07036	1 copy
University of Maryland Department of Physics and Astronomy Attn: D. Currie College Park, MD 20742	1 copy
Sylvania Electric Products, Inc. Attn: L. M. Osterink 100 Fergeson Drive Mountain View, CA 94040	1 copy
North American Rockwell Corp. Autonetics Division Attn: R. Gudmundsen 3370 Miraloma Avenue Anaheim, CA 92803	1 copy
Massachusetts Institute of Technology Attn: Prof. A. Javan 77 Massachusetts Avenue Cambridge, MA 02138	1 copy

Lockheed Missile & Space Co. | 1 copy
Attn: Dr. R. C. Ohlman
Palo Alto Research Laboratories
Palo Alto, CA 94304

ILC Laboratories, Inc. | 1 copy
Attn: L. Noble
164 Commercial Street
Sunnyvale, CA 94086

University of Texas at Dallas | 1 copy
Attn: Prof. Carl B. Collins
P. O. Box 30365
Dallas, TX 75230

Polytechnic Institute of New York | 1 copy
Attn: Dr. William T. Walter
Rt. 110
Farmingdale, NY 11735